Effects of Boundary Conditions on Magnetic Friction

Kentaro Sugimoto

Department of Physics, The University of Tokyo

January 1, 2018

I would like to express my deepest gratitude to Prof. Naomichi Hatano, whose enormous support and insightful comments were invaluable during the course of my study. I am also indebt to Dr. Ryo Tamura who provided technical help and sincere encouragement. I would also like to express my gratitude to my family for their moral support and warm encouragements.

Enumerate those who encouraged my research.

Abstract

In the present thesis, hogehoge. Moreover, fugafuga.

Todo list

Contents

Chapter 1

Introduction

In this chapter we introduce two of the most famous problems in analyzing the frictional force as problems of statistical mechanics. We give recent developments for solving these problems. We then pose another problem regarding *manipulation* of the sliding friction which occurs in highly lubricated solids. To this end we simplify our problem into a dimensional crossover in lattice systems.

The sliding friction in solids is a very complicated problem to analyze, despite the fact that our daily lives are linked with it in various forms. One reason of the difficulty is that there is no general theory which determines the most important microscopic degree of freedom to describe the macroscopic phenomenon of the sliding friction.

One may think that with the skill of statistical mechanics we can deal with the problem in a systematic manner. However, there are several essential problems including the following: (i) The sliding friction is essentially a non-equilibrium phenomenon (see Section 1.1); (ii) We cannot directly observe the sliding surface (see Section 1.2).

1.1 Sliding Frictions as Non-Equilibrium Problems

We can regard the sliding friction as the following elementary problem. We consider an object O and a substrate S, and let S slide against O by applying an external force $f_{\rm ext}$ to O. When O and S interact with each other, the kinetic energy of O given by the external force is expected to be lost through the interaction, and then the entire system $O + S$ heats up (if the system is closed) or the energy dissipates from the system to an external environment (if the system is open). In the latter case, when we control the external force $f_{\rm ext}$ to balance it with the frictional force $f_{\rm fric}$ the sliding velocity v becomes constant and the dissipation process becomes stationary. Then the frictional force $f_{\rm fric}$ can be considered as a function of the sliding velocity.

The standard method of the statistical mechanics called the linear-response theory appears to solve the problem if the velocity is much smaller than the rate ξ/τ, where ξ and τ are the characteristic length and time of the system, respectively. However, we already know well that the static frictional force is non-zero for several systems, for which the frictional force has a non-linear velocity dependence. This shows us that the complexity of the problem is beyond the linear-response theory.

Several model calculations and experiments have solved these problems, directlyCite! or indirectlyCite!. Phononic contributions to sliding frictions were analyzed with the Frenkel-Kontorova model [1–7] and simulated with cold atoms [8–10], whereas eletronic contributions were discovered [11] and explained within an image potential theory [12]. As a quantum phenomena, sliding friction between adsorbed helium atoms and its substrates [13–15] is recently getting attention, but their theoretical description is still not satisfactory and remains to be an open problem.

1.2 Impossibility of the Observation of the Sliding Surface

The dimensionality of the sliding surface is up to two, if that of the whole system is three. Sliding surfaces are different in many ways from the standard two-dimensional surfaces on three-dimensional solids which have been investigated for many years. In particular we cannot perform a direct observation of the sliding surface by apparatuses such as microscopes. The difficulty prevents us from clarifying non-equilibrium properties of the sliding friction.

The frictional-force microscope have played important roles is investigating such sliding surfaces. This apparatus sees the roughness of the substrate by observing frictional force on its tips, by which we can recover the macroscopic frictional force as its integration over the area of surface. By the use of frictional-force microscopes a local lateral force was measured by Ternes *et al.* [16] and *superlubricity* was observed by Urbakh [17] as an intriguing phenomena that the frictional force is strongly dependent on the sliding direction and almost vanishes in several directions.

1.3 Manipulating the Friction

As mentioned above, recent researches well revealed the nature of sliding frictions. This gave rise to new problems about the friction in atomically microscopic systems.

Ordinary frictions in solids are mostly governed by excitations of phonon degrees of freedom, because the sliding surface is almost always rougher than the scale of the atom. Once we lubricate the sliding surface highly, other degrees of freedom such as the orbital and the spin angular momenta of electrons emerge as additional contributions to the friction.

We are already familiar with the most remarkable example of such a system in our daily

lives, namely *micro electric mechanical systems* (**MEMS**). MEMS plays important roles in the printing head of inkjet printers, the accelerometer in smartphones and so on. MEMS has clean planes sliding with an accuracy of a micrometer or a nanometer [18–20], because of which they experience the friction with many kinds of degrees of freedom including not only phonon excitations but also other contributionsConcrete Exmaples!. The small size of these systems results in a large friction, which lessens the working efficiency or disables the operation of MEMS, because the ratio of the surface area over the volume of the system becomes larger with the smaller size and a fixed geometry. In order to tackle with the issue of manipulation of the friction in small systems, we need to obtain more fundamental knowledge of the friction.

1.4 Magnetic Friction

The way to manipulate the friction in small systems is less understood than its nature. We here consider manipulation of magnetic materials by numerically simulating lattice models.

The nature of magnetic frictions was first revealed by Kadau *et al.* [21] by the use of the Ising model. Just after it, Fusco *et al.* investigated magnetic frictions in Heisenberg spin systems and a moving dipole moment on them. A crossover of the velocity dependence on the magnetic frictional force was revealed by Magiera *et al.* [22]. A direct observation of magnetic frictions by a scanning probe microscopy was then performed by Wolter *et al.* [23].

In the present work we consider two strips of the quasi-one-dimensional Ising model sliding against each other with a fixed velocity. We discuss the difference of the frictional forces for the two boundary conditions, the anti-parallel and the parallel, and its dependence on the distance between the two boundaries.

Based on the results in Ref. [24], we consider a dimensional crossover from one dimension to two in Ising models with two fixed boundary conditions. In the one-dimensional limit

the boundary conditions seem to have the maximum effect on the friction, whereas in the two-dimensional limit there seems to be no effects. Behaviors in the both limits for the free boundary conditions correspond to the results in Ref. [24]. We find a method of manipulating the friction using different boundary conditions. These boundary conditions can be realized in experiments by aligning the boundary spins of sliding magnets.

Frictions in such models were considered first in a numerical study by Kadau *et al.* [21]. They revealed by Monte Carlo simulations that two square lattices of the Ising model which slide against each other experience the friction, depending on the temperature and the sliding velocity. Immediately after the research, it was revealed [24] that the Ising model goes under a non-trivial non-equilibrium phase transition (**NEPT**) in the high-velocity limit, where the two square lattices are decoupled in terms of the correlation between the two lattices and feel an effective mean field depending on the magnetization of each other [24]. This analysis showed that a novel critical point which is located at a generally higher temperature than the ordinal critical point for models in arbitrary dimensions and geometries (see Chapter 2). They also developed a new dynamics [24] which enables an analytical treatment for finite sliding velocities, obtaining a non-equilibrium critical line.

Chapter 2

Velocity-driven Non-equilibrium Phase Transition in Ising Models

To discuss the non-equilibrium crossover between two different dimensionalities, we make a brief review of the exact results [24] by Hucht. His analysis is based on the fact that two Ising cylinders with relative motion make a novel mean field, which leads the system to a non-trivial phase transition.

Let us consider two equivalent square lattices of the Ising model each of which contacts the other by one of its one-dimensional boundaries (see Fig. 2.1). We make one lattice slide along the contact plane against the other lattice with a constant velocity v. The entire system thereby goes into a non-equilibrium stationary state instead of equilibration. The non-equilibrium stationary state well describes the behavior of two magnetic materials with a friction. This setup is explained in detail in Chapter 3.

As a well known fact, the ordinary two-dimensional Ising model has an equilibrium phase transition at the critical temperature $T_{\mathrm{c,eq}} = 2/(\log\left[1+\sqrt{2}\right])$ in the thermodynamical limit. The system with the friction becomes equivalent to the equilibrium case in the limit of $v \to 0$. In

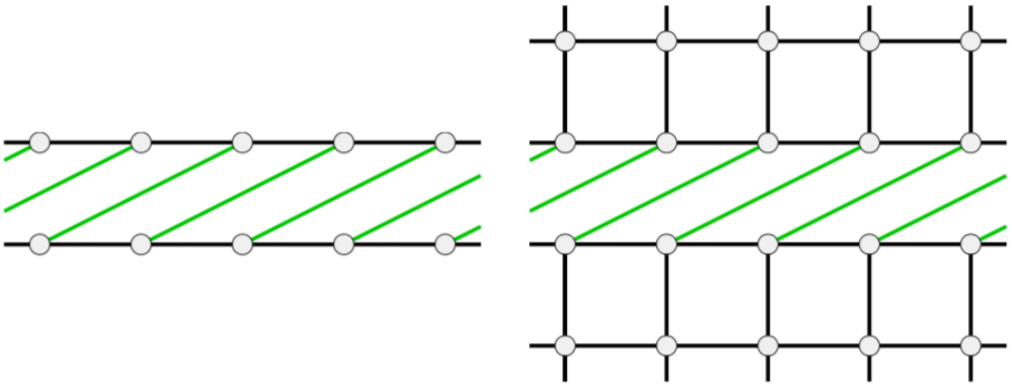

(a) (b)

Figure 2.1: Sketches of the models considered in Ref. [24]. Both cases depict a schematic view after the sliding by twice a lattice constant. (a) Two chains of the one-dimensional model. (b) Two lattices of the two-dimensional model.

addition to the ordinary phase transition, a novel phase transition in which the magnetization grows on the sliding boundary (see Fig. 2.2). Now we denote the velocity dependent non-equilibrium critical point by $T_c(v)$ apart from the equilibrium critical point $T_{\mathrm{eq,c}}$. Hucht [24] claims that the critical temperature $T_c(v)$ *deviates* from $T_{\mathrm{c,eq}}$ at the point $v = 0$ towards the limit $v = \infty$.

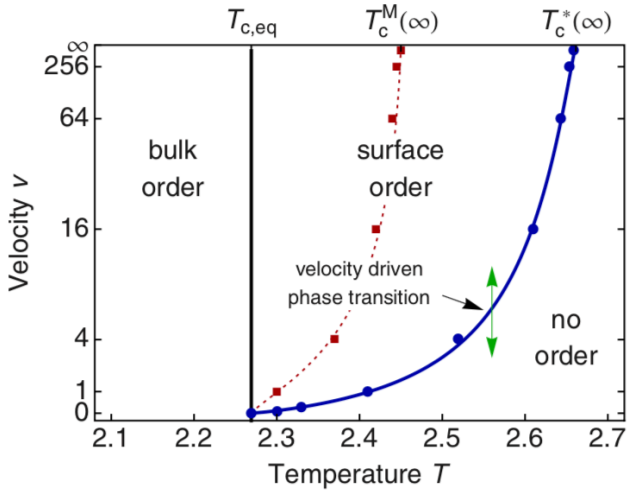

Figure 2.2: The phase diagram of the two-dimensional non-equilibrium Ising model [24]. The black solid line, the red dashed line and the blue solid line indicate the ordinary bulk phase transition, a non-equilibrium boundary phase transition for the Metropolis rate and the multiplicative rate, respectively. From right to left across the non-equilibrium phase boundary the system acquires non-zero expectation value of magnetization on the sliding boundary.

This phenomenon wes first reported in the numerical results [21] by Kadau *et al.* using Monte

Carlo simulations both on the Metropolis and the Glauber algorithms in a two-dimensional model, and then was investigated in a more analytic manner [24] by Hucht in several dimensionalities and model geometries. One of the important points of the latter result is that in the limit $v \to \infty$ we can write down a closed exact equation for the *second* critical temperature $T_c^*(\infty)$. It is also important that a novel algorithm called *multipricative rate* enabled us to give an equation of $T_c^*(v)$, which depends on the flip rate and the sliding velocity $v > 0$.

If the velocity v is much less than the rate $\xi_x^{(\mathrm{eq})}(\beta)/\tau_x^{(\mathrm{eq})}(\beta)$, we can expect the system to behave similarly to its equilibrium state, where $\xi_x^{(\mathrm{eq})}(\beta)$ and $\tau_x^{(\mathrm{eq})}(\beta)$ are the correlation length along the direction parallel to the sliding surface and the correlation time, respectively, for the equilibrium state at an inverse temperature $\beta := (k_{\mathrm{B}}T)^{-1}$. This corresponds to the case in which the pumped energy by the constant sliding quickly relaxes into the heat bath and the structure of domain walls near the sliding boundary is well sustained. On the other hand, the velocity v much greater than the rate $\xi_x^{(\mathrm{eq})}(\beta)/\tau_x^{(\mathrm{eq})}(\beta)$ should lead the system to a stationary state far from equilibrium, so that the structure near the sliding boundary is destroyed.

In the latter case a mean field picture well describes the behavior of the system; a set of the moving spins along the contact plane act on the other set of *relatively* moving spins as a spatially averaged effective field. This view enables us to write a self-consistent equation for the temperature $T_c(\infty)$.

We summarize the result for one-dimensional chains and two-dimensional planes in order to discuss the crossover from one dimension to two dimensions in our models in Chapter 5. We first give a general Hamiltonian of the Ising model as follows.

$$\beta\mathcal{H}_\mu := -K\sum_{i<j}\sigma_i\sigma_j - h^{\mathrm{ext}}\sum_i \sigma_i - \sum_i k_i\mu_i\sigma_i, \tag{2.1}$$

where K, $h^{\rm ext}$ and $k_i\mu_i$ denote the exchange interaction, the external field and the stochastic field on the ith spin ($\mu_i = \pm 1$), respectively. The geometry of the model is either Fig. 2.1 (a) or (b). Now we assume that μ_i obeys a probability distribution $p_i(\mu_i)$ such that $\langle \mu_i \rangle := \sum_{\mu_i=\pm 1} p_i(\mu_i)\mu_i = m_i$ for a given value of m_i. The form $p_i(\mu_i) := (1+\mu_i m_i)/2$ actually satisfies the condition.

If we decompose the Hamiltonian into the contribution of the stochastic field and the rest as

$$\beta\mathcal{H}_\mu = \beta\mathcal{H}_0 - \sum_i k_i\mu_i\sigma_i, \tag{2.2}$$

where

$$\beta\mathcal{H}_0 := -K\sum_{i<j}\sigma_i\sigma_j - \sum_i h_i^{\rm ext}\sigma_i, \tag{2.3}$$

the partition function of the system is written in the form

$$\mathcal{Z} = \left\langle {\rm Tr}_\sigma \left[{\rm e}^{-\beta\mathcal{H}_\mu} \right] \right\rangle = {\rm Tr}_\sigma \left[{\rm e}^{-\beta\mathcal{H}_0} \left\langle \prod_i {\rm e}^{k_i\mu_i\sigma_i} \right\rangle \right] \tag{2.4}$$

$$= \prod_j \cosh k_j \ {\rm Tr}_\sigma \left[{\rm e}^{-\beta\mathcal{H}_0} \prod_j (1+\sigma_i m_i \tanh k_i) \right]. \tag{2.5}$$

Owing to the translation invariance along the sliding direction, we assume a homogeneous boundary magnetization $m_i = m_{\rm b}$ for all boundary sites i. Each boundary magnetization acts as an effective field $h_{\rm b}$ on the other boundary magnetization.

The model therefore reduces to

$$\beta\mathcal{H}_{\rm eq} := -K\sum_{i<j}\sigma_i\sigma_j - h_{\rm b}\sum_i \sigma_i = \beta\mathcal{H}_0 - \sum_i b\sigma_i, \tag{2.6}$$

with $b := h_{\rm b} - h^{\rm ext}$, which relaxes toward the equilibrium state. Its partition function is written as

$$\mathcal{Z}_{\rm eq} = {\rm Tr}_\sigma\left[{\rm e}^{-\beta\mathcal{H}_{\rm eq}}\right] = {\rm Tr}_\sigma\left[{\rm e}^{\beta\mathcal{H}_0}\sum_i {\rm e}^{b\sigma_i}\right] \tag{2.7}$$

$$= \prod_i \cosh b\ {\rm Tr}_\sigma\left[{\rm e}^{-\beta\mathcal{H}_0}\prod_i(1+\sigma_i\tanh b)\right]. \tag{2.8}$$

Comparing the right-hand sides of Eqs. (2.5) and (2.8), we have $\mathcal{Z} \propto \mathcal{Z}_{\rm eq}$ if it holds that $\tanh b = m_{\rm b}\tanh k_i$.

Our model gives the strength of the stochastic field k_i as the exchange interaction across the sliding surface K, and thus it holds that $k_i = K$ and

$$h_{\rm b} = \tanh^{-1}\left(m_{\rm b}\tanh K\right), \tag{2.9}$$

in the limit $h^{\rm ext} \to 0$. The boundary magnetization under a static field $h_{\rm b}$ has a form of

$$m_{\rm b,eq}(K, h_{\rm b}) := \frac{\partial}{\partial h_{\rm b}}\mathcal{Z}_{\rm eq}, \tag{2.10}$$

and thus we have

$$m_{\rm b,eq}\left(K, \tanh^{-1}\left(m_b\tanh K\right)\right) = m_b \tag{2.11}$$

as a self-consistent relation for m_b. The critical point is given by

$$1 = \left. \frac{\partial m_{\mathrm{b,eq}}}{\partial m_{\mathrm{b}}} \right|_{m_{\mathrm{b}}=0}. \tag{2.12}$$

Expanding the left-hand side of Eq. (2.11) to the first order of m_{b} and using the condition (2.12) we have

$$m_{\mathrm{b,eq}}\left(K, 0\right) + m_b \tanh\left(K\right) \left. \frac{\partial m_{\mathrm{b,eq}}}{\partial h_{\mathrm{b}}} \right|_{h_{\mathrm{b}}=0} = m_b. \tag{2.13}$$

With the definition of the equilibrium susceptibility $\chi_{\mathrm{b,eq}}(K) := \partial m_{\mathrm{b,eq}}/\partial h_{\mathrm{b}}|_{h_{\mathrm{b}}=0}$ and the fact $m_{\mathrm{b,eq}}\left(K, 0\right) = 0$, we finally have

$$\tanh\left(K\right) \chi^{(0)}_{\mathrm{b,eq}}(K) = 1. \tag{2.14}$$

The condition (2.14) determines the non-equilibrium critical temperature $K = K_{\mathrm{c}}$. Using the expression of the magnetization for the one-dimensional Ising model and the boudnary magnetization for the two-dimensional model, we have the numerical solutions of the condition (2.14) as

$${K_{\mathrm{c}}}^{-1} = \begin{cases} 2.2691853\ldots & \text{in one dimension,} \\ 2.6614725\ldots & \text{in two dimensions.} \end{cases} \tag{2.15}$$

Note that the temperature K_{c} corresponds to the non-equilibrium critical temperature in the limit $v \to \infty$, and is consistent to the extrapolation from the results for two dimensions with the multipricative rate (see Fig. 2.2).

Chapter 3

Numerical Simulations

3.1 Setup of the Model

Sliding friction is a form of energy dissipation on the surface between a moving object and its substrate. The dissipated energy is originated in the kinetic energy of the moving object. We here consider a constantly moving case in which an external force maintains the motion of the object with endless supply of its kinetic energy. This view leads to its *non-equilibrium stationary state*. When the system is in a non-equilibrium stationary state, it is often easy to calculate *energy currents* such as the frictional heat, its power and so on. Applying the view to our case in which two square lattices of the Ising model slide against each other, we can formulate the problem as follows; see Fig. 3.1.

1. We prepare a square lattice of the Ising model of size $L_x \times L_z$ and impose periodic boundary conditions in the transverse (x) direction. We first set the system in the equilibrium state of a temperature T, whereas we set the open boundary conditions in the longitudinal (z) direction for the moment.

2. We cut the system along the x-direction into two parts, maintaining interactions on the

cut.

3. We slide two parts along the cut plane with relative velocity v. In other words, we shift the upper half by a lattice constant every $1/v$ unit time.

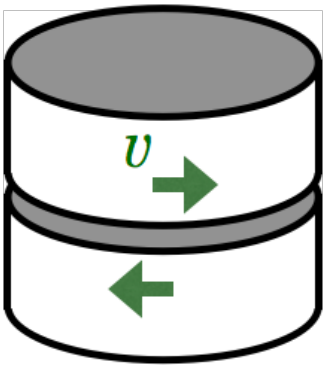

Figure 3.1: Two cylinders of the Ising model sliding with the velocity v.

The Hamiltonian of the system is given by

$$\hat{H} = \hat{H}_{\text{upper}} + \hat{H}_{\text{lower}} + \hat{H}_{\text{slip}}(t), \tag{3.1}$$

where

$$\hat{H}_{\text{upper}} := -J \sum_{\langle i,j \rangle \in \text{upper}} \hat{\sigma}_i \hat{\sigma}_j, \tag{3.2}$$

$$\hat{H}_{\text{lower}} := -J \sum_{\langle i,j \rangle \in \text{lower}} \hat{\sigma}_i \hat{\sigma}_j, \tag{3.3}$$

$$\hat{H}_{\text{slip}}(t) := -J \sum_{\langle i,j(t) \rangle \in \text{slip}} \hat{\sigma}_i \hat{\sigma}_{j(t)} \tag{3.4}$$

upper, lower and slip representing the set of interacting spin pairs on the upper half, the lower half and the slip plane, respectively. Shift operations lead the system to repeated *pumping* and *dissipation* processes as follows:

1. **Shift**: A shift operation excites the energy on the slip plane by the amount $\langle \hat{H}_{\text{slip}}(t') -$

$\hat{H}_{\rm slip}(t)\rangle_{\rm st}$. The letter t' denotes the time just after the shift operation at time t.

2. **Relax-1**: The excited energy on the slip plane $\langle \hat{H}_{\rm slip}(t') - \hat{H}_{\rm slip}(t)\rangle_{\rm st}$ dissipates to the entire system.

3. **Relax-2**: The excited entire system relaxes towards the equilibrium.

We defined the stationary state average $\langle \hat{A}\rangle_{\rm st} := \sum_i A_i p_i^{\rm (st)}$ for an arbitrary observable $\hat{A}$, where $\{A\}_i$ are eigenvalues of $\hat{A}$ and $\{p_i^{\rm (st)}\}$ is the stationary-state probability distribution, which is different from the equilibrium (canonical) probability distribution $p_i^{\rm (eq)} \propto \exp\left[-E_i/k_{\rm B}T\right]$. Note that the distribution $\{p_i^{\rm (st)}\}$ depends on the sliding velocity v.

The excited and relaxed amounts of energy per unit time correspond to the energy pumping and dissipation, respectively. The energy pumping $P(t)$ and dissipation $D(t)$ are given by

$$P(t) := \sum_{i_v=0}^{v-1} \left\langle \hat{H}_{\rm slip}\left(t' - 1 + \frac{i_v}{v}\right) - \hat{H}_{\rm slip}\left(t - 1 + \frac{i_v}{v}\right)\right\rangle_{\rm st}, \tag{3.5}$$

$$D(t) := \sum_{i_v=0}^{v-1} \left\langle \hat{H}_{\rm slip}\left(t - 1 + \frac{i_v+1}{v}\right) - \hat{H}_{\rm slip}\left(t' - 1 + \frac{i_v}{v}\right)\right\rangle_{\rm st}, \tag{3.6}$$

respectively. $P(t)$ and $D(t)$ correspond to the energy difference due to the **Shift** and the **Relax** processed, respectively. Note that absolute values of $P(t)$ and $D(t)$ become equal to each other in the non-equilibrium stationary state, by its definition.

3.2 Definitions of Physical Quantities

We now consider the case in which the system is in a non-equilibrium stationary state. We denote by $P(L_x, L_z, T)$ and $D(L_x, L_z, T)$ the long-time limit of energy pumping $P(t)$ and dissipation $D(t)$ for a system of size $L_x \times L_z$ at the temperature T. We define the frictional force

density $f(L_z, T)$ by

$$f(L_z, T) := \lim_{L_x \to \infty} \frac{F(L_x, L_z, T)}{L_x}. \tag{3.7}$$

In numerical simulations, we calculate the frictional force $F(L_x, L_z, T)$ using its power $D(L_x, L_z, T)$ by the formula

$$F(L_x, L_z, T) = \frac{D(L_x, L_z, T)}{v}. \tag{3.8}$$

We can easily verify the formula (3.8) by considering general cases in which the frictional force and its power are both time dependent. Denoting the frictional force $F(x)$ at the position x, it holds that

$$\int_{t_0}^{t_1} dt\ D(t) = \int_{x(t_0)}^{x(t_1)} dx\ F(x) = \int_{t_0}^{t_1} \frac{dx}{dt} dt\ F(x(t)) = v \int_{t_0}^{t_1} dt\ F(x(t)) \tag{3.9}$$

for a time dependent $D(t)$, because $dx/dt = v$. Under the assumption of a non-equilibrium stationary state, the integrands in both-hand sides of the relation (3.9) are still equal to each other in the long-time limit, and hence

$$D(L_x, L_z, T) = vF(L_x, L_z, T). \tag{3.10}$$

From now we call the quantity $D(L_x, L_z, T)$ the *energy dissipation*.

Our model always reaches a non-equilibrium stationary states in the long-time limit $t \to \infty$, which depends on the temperature T and the sliding velocity v; We will prove it in . A. We use the fact that $\lim_{t\to\infty} |D(t)| = \lim_{t\to\infty} |P(t)|$ in order to estimate the average $\bar{D}$; the average $\bar{P}$

has less statistical fluctuation [22, 25, 26]. We therefore have

$$P(L_x, L_z, T) = vF(L_x, L_z, T). \tag{3.11}$$

We also define the bulk energy density $\epsilon_{\rm b}(L_z, T)$ as follows:

$$\epsilon_{\rm b}(L_z, T) := \lim_{L_x \to \infty} \frac{E_{\rm b}(L_x, L_z, T)}{L_x L_z}, \tag{3.12}$$

where $E_{\rm b}(L_x, L_z, T)$ is the energy of the entire system. From this, we define the bulk heat capacity $c_{\rm b}(L_z, T)$ as follows:

$$c_{\rm b}(L_z, T) := \frac{\partial \epsilon_{\rm b}(L_z, T)}{\partial T}. \tag{3.13}$$

3.3 Non-equilibrium Monte Carlo Simulation

The dissipation process towards the heat bath occurs via a spin flip. This fundamental processes do not only describe equilibrium states but also non-equilibrium stationary states at a fixed temperature T [27]. Using Monte Carlo method, we simulate this process.

3.3.1 Introduction the Time Scale to Ising Models

In order to calculate dynamical observables such as the frictional power (3.11) and its dissipation rate (3.8), we have to define *a unit time* for finite size systems.

For the equilibrium Monte Carlo simulation, the most naive approach for the equilibrium state is the single-spin-flip algorithm, where we perform the sequence of a random selection of a spin and its flip with a temperature dependent probability $p(T)$. Whatever we use as

the probability for the Monte Caro simulation should satisfy a good property, called *detailed balanced condition*, which certainly leads the system towards the true equilibrium state with enough repetition of the sequence. For example, we often use the Metropolis probability $p_{\mathrm{M}}(T) := \min\{1, \mathrm{e}^{-\frac{\Delta E}{k_{\mathrm{B}}T}}\}$ as the probability $p(T)$, where ΔE is the energy difference due to the flip. We often call a *Monte Carlo step* a single process of the algorithm, and define a *Monte Carlo sweep* by N Monte Carlo steps, where N is the number of spins.

Which do we have to define a unit time by a Monte Carlo step or a Monte Carlo sweep? Its answer can be seen in the following manner: We often assume that a statistical mechanical model are coupling to a heat bath by each local degree of freedom. The temperature of the system is kept constant by the heat bath and exchanges its energy with the heat bath through local degrees of freedom. It is most natural to assume that the frequency of the exchanging process is dependent only on the temperature of the heat bath. Thus the total number of times exchanged are proportional to the number of degrees of freedom of the system. It is justified to define a unit time by a Monte Carlo sweep. Note that the more spins the system contains, the higher time resolution we can simulate with.

3.3.2 Slip Plane with the Velocity v

Using the introduced time scale, we can also introduce the slip plane with the velocity v to the system with N spins. Corresponding to the setup in Sec. 3.1, we perform an extended single-spin-flip algorithm as follows:

1. **Shift**: We shift the upper half of the lattice by a lattice constant.

2. **Flip**: We perform ordinary single flips for N/v times.

3. We repeat the processes 1 and 2 for v times.

In the extended algorithm, the upper half slides with the velocity v in a unit time at regular intervals. We proved the fact that this algorithm leads the system of any size to a non-equilibrium stationary state depending on the temperature T and the velocity v (see App. A for details).

3.3.3 Calculation Method

The observables that we are interested in are the frictional power $P(t)$ and its dissipation rate $D(t)$. In Monte Carlo simulations, they are the energy difference for a unit time due to the shift and the flip operation, respectively. Both observables have the same absolute value in the long-time limit.

Chapter 4

Results

In this chapter, we first prove that the Monte Carlo simulation necessarily converges to a NESS from arbitrary initial conditions by a view of stochastic matrices and that the NESS depends only on the temperature T and the sliding velocity v. We next show the results of Monte Carlo simulations of the Ising models. To discuss the dependence of the frictional force density $f(L_z, T)$ and the bulk energy density $\epsilon_{\rm b}(L_z, T)$ on the size L_z and the temperature T with the fixed velocity $v = 10$, we performed the numerical large size limit $L_x \to \infty$ with the fixed L_z and T (see Sec. 4.2.4). To get the observables in the non-equilibrium stationary state, we performed the equilibration process for 5000 sweeps and the stationarization process for 5000 sweeps for all given parameters. The convergence of the observables to the equilibrium value and the stationary value for these time regions respectively are checked carefully.

The range of parameters in our simulation is as follows. We computed the value of $f(L_z, T)$ for temperatures $k_{\rm B}T/J \in \{0.0, 0.1, 0.2, \ldots, 1.9, 2.0, 2.02, 2.04, \ldots, 2.48, 2.50, 2.6, 2.7, \ldots, 5.0\}$ and sizes $L_z \in \{4, 6, 8, 10, 12, 14, 16, 32, 64\}$ with the two boundary conditions, the anti-parallel and the parallel. For the anti-parallel boundary the initial state is set to the domain-wall state, where spin variables σ_i in the upper half of the system are the same value as the upper

boundary, and in the lower half as the lower boundary. For the parallel boundary the initial state is set to the magnetized state, where all spin variables σ_i are the same value as both of boundaries. The reason why we used these initial states is that they are the most natural ground states which correpond to each of the boundary conditions.

All the simulations are performed by the single flip algorithm with the Metropolis rate. We performed these simulations for 480 samples for all parameters and averaged them, and then averaged along the time direction.

In addition, we also show their temperature derivatives to discuss the phase transitions.

4.1 Stochastic Matrices and Non-Equilbrium Monte Carlo Simulations

We prove that our Monte Carlo simulations converges to a NESS with the Metropolis rate. The result below can be easily generalized to cases with an arbitrary rate. We construct the following stochastic matrix, which corresponds to a Monte Carlo sweep in the model with magnetic friction:

$$\hat{T}(\beta, v) := \left[\left\{ \hat{M}(\beta) \right\}^{V/v} \hat{S} \right]^{v}, \tag{4.1}$$

where $v \in \{\text{Divisors of } V\}$ and $V := L_x \times L_z$. The matrix $\hat{M}(\beta)$ and $\hat{S}$ express a Monte Carlo step at a temperature T and sliding the upper-half by a lattice constant, respectively for the model of size $L_x \times L_z$. The matrix $\hat{T}(\beta, v)$ describes a time evolution for a Monte Carlo sweeps, because the matrix have the V/vth power of $\hat{M}(\beta)$. The matrix $\hat{M}(\beta)$ and $\hat{S}$ also have a sparse structure and the structure similar to the unit matrix, respectively (see Figs. 4.1a, 4.1b). Note

that corresponding to the dense structure of the matrix $\left\{\hat{M}(\beta)\right\}^{V}$, the matrix $\hat{T}(\beta, v)$ is also dense; see Fig. 4.1c.

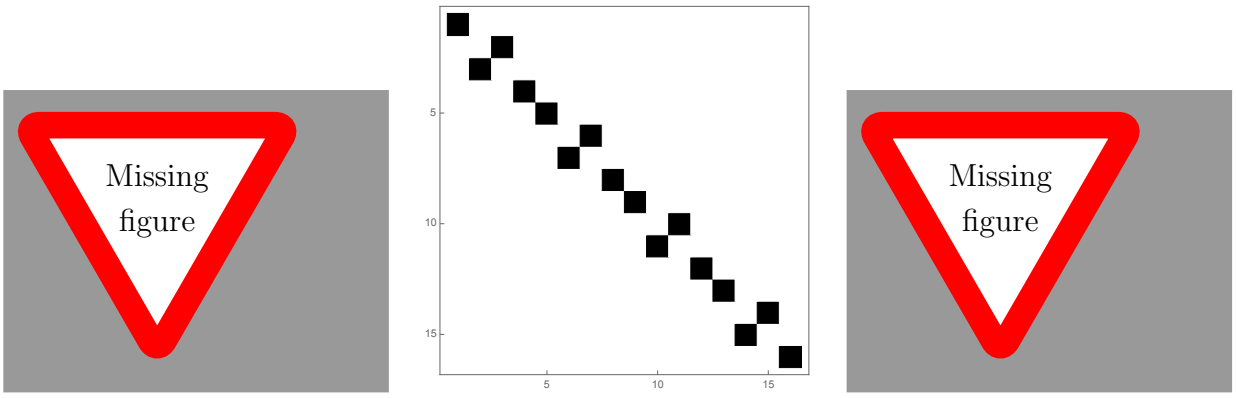

(a) (b) (c)

Figure 4.1: Array plots of matrices for the model of size $L_x = 2, L_z = 2$ and at the temperature $\beta = 0.1$. (a) $\hat{M}(\beta)$. (b) $\hat{S}(\beta)$. (c) $\hat{T}(\beta, v)$

The task of diagonalizing the Matrix $\hat{T}(\beta, v)$ is the same as that of $\left\{\hat{M}(\beta)\right\}^{V/v} \hat{S}$, which corresponds to a time evolution for $1/v$ Monte Carlo sweeps. We show eigenvalue distributions of $\left\{\hat{M}(\beta)\right\}^{V/v}$ and $\left\{\hat{M}(\beta)\right\}^{V/v} \hat{S}$ for the model of size $L_x = 2, L_z = 2$ (see Figs. 4.2a, 4.2b). These eigenvalue distributions are similar to each other, reflecting that both of them correspond to a time evolution for $1/v$ Monte Carlo sweeps.

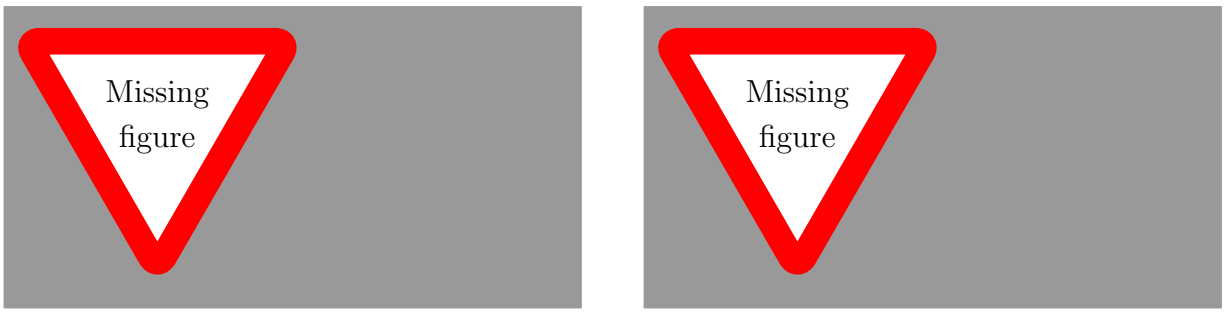

(a) (b)

Figure 4.2: Eigenvalue distributions of matrices for the model of size $L_x = 2, L_z = 2$ and at the temperature $\beta = 0.1$. (a) $\left\{\hat{M}(\beta)\right\}^{V/v}$. (b) $\left\{\hat{M}(\beta)\right\}^{V/v} \hat{S}$.

4.2 Non-equilibrium Monte Carlo Simulations

4.2.1 Frictional Force Density $f(L_z, T)$

We show the behavior of the frictional force density $f(L_z, T)$ (see Fig. 4.3). For both boundary conditions, the anti-parallel and the parallel, extremely smaller sizes such as $L_z = 4, 6$ make greater differences from its value for the current maximum size $L_z = 64$, where an asymptotic behavior emerges. We can expect that for more larger sizes such as $L_z = 128, 256, \ldots$ makes no longer great differences from that of $L_z = 64$, thus we can say that the system reaches *two-dimension* in the vicinity of the size $L_z = 16$.

An additional important aspect is the difference between the values for anti-parallel and the parallel boundary conditions. In the former case, the smaller size L_z makes the greater value of the frictional force density $f(L_z, T)$. On the other hand, the latter case indicates the reverse behavior that smaller size L_z makes the smaller value of the frictional force density $f(L_z, T)$. This physical meaning is that the size L_z and the correlation length of the system along the z-direction $\xi_z(\beta)$ become comparable, and then the system behaves as the one-dimension for the smaller size L_z, whereas much greater size L_z than the correlation length $\xi_z(\beta)$ makes the system two-dimensional. Note that for $L_z = 64$ behaviors for both cases are similar to each other and we can expect that these behaviors reach to the results by Kadau [21].

4.2.2 Bulk Energy Density $\epsilon_{\mathrm{b}}(L_z, T)$

We show the behavior of the bulk energy density $\epsilon_{\mathrm{b}}(L_z, T)$ (see Figure 4.4). As same as frictional force densities $f(L_z, T)$, bulk energy densities $\epsilon_{\mathrm{b}}(L_z, T)$ indicates an asymtotic behavior.

In the anti-parallel case, the smaller size L_z makes the system well disorder. On the other hand, the parallel case indicates no drastic change driven by the smaller size L_z.

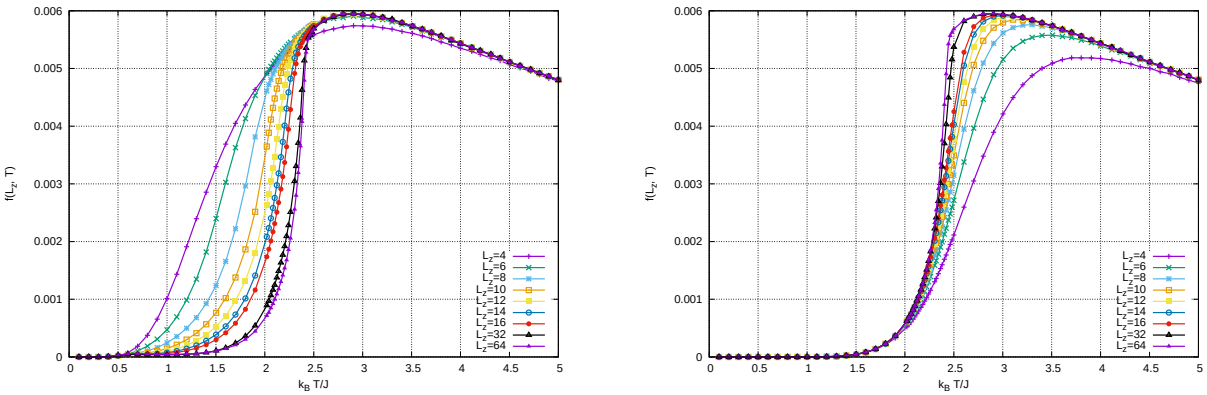

(a) (b)

Figure 4.3: Temperature dependences of $f(L_z, T)$ with each boundary condition. (a) The anti-parallel boundary. (b) The parallel boundary.

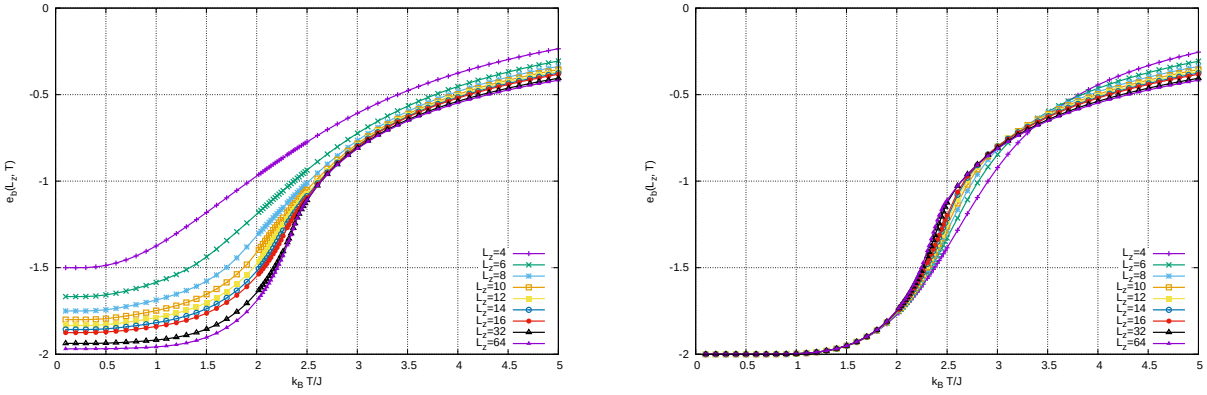

(a) (b)

Figure 4.4: Temperature dependences of $\epsilon_{\mathrm{b}}(L_z, T)$ with each boundary condition. (a) The anti-parallel boundary. (b) The parallel boundary.

4.2.3 Temperature Derivatives $\partial f(L_z,T)/\partial T$, $\partial \epsilon_{\rm b}(L_z,T)/\partial T$

We additionally show the behavior of temperature derivatives $\partial f(L_z,T)/\partial T$, $c_{\rm b}(L_z,T) = \partial \epsilon_{\rm b}(L_z,T)/\partial T$ (see Fig. 4.5, 4.6).

Both of them exhibit sharp peak at characteristic temperatures, respectively the crossover-driven divergence at a characteristic temperature near $T = 2.40$ for both boundary conditions for the largest size $L_z = 64$. This imply that these diverge for the limit of $L_z \to \infty$. If we regards the peak $T_{\rm peak}(L_z)$ as the pseudo critical point, where $\partial^2 f(L_z,T)/\partial T^2|_{T=T_{\rm peak}(L_z)} = 0, \partial^2 \epsilon_{\rm b}(L_z,T)/\partial T^2|_{T=T_{\rm peak}(L_z)} = 0$, we can recognize the shift of peaks toward the higher temperature for the anti-parallel boundary, whereas peaks shifts toward the lower for the parallel boundary. These describes the effects of the boundary condition which acts on the system as an effective field, and the effects are enhanced by the smaller L_z. Namely the anti-parallel boundary acts as a demagnetizing field such that the pseudo critical point $T_{\rm peak}(L_z)$ shifts toward the lower, and the parallel boundary acts as a magnetizing field such that the pseudo critical point $T_{\rm peak}(L_z)$ shifts toward the higher.

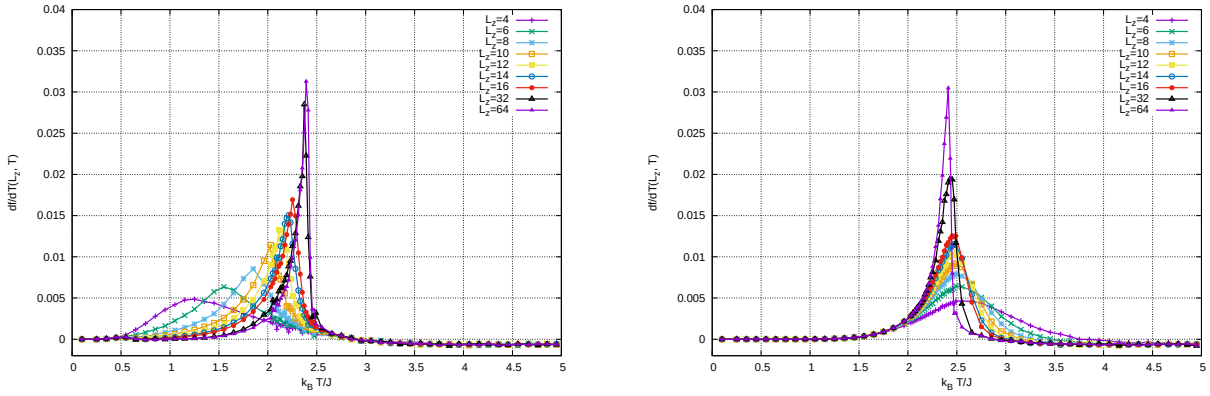

(a) (b)

Figure 4.5: Temperature dependences of $\partial f(L_z,T)/\partial T$ with each boundary condition. (a) The anti-parallel boundary. (b) The parallel boundary.

The frictional force density $\partial f(L_z,T)/\partial T$ and the bulk energy density $\epsilon_{\rm b}(L_z,T)/\partial T$ exhibit an asymptotic and divergent behavior to a function of temperature T, and its peak near $T =$

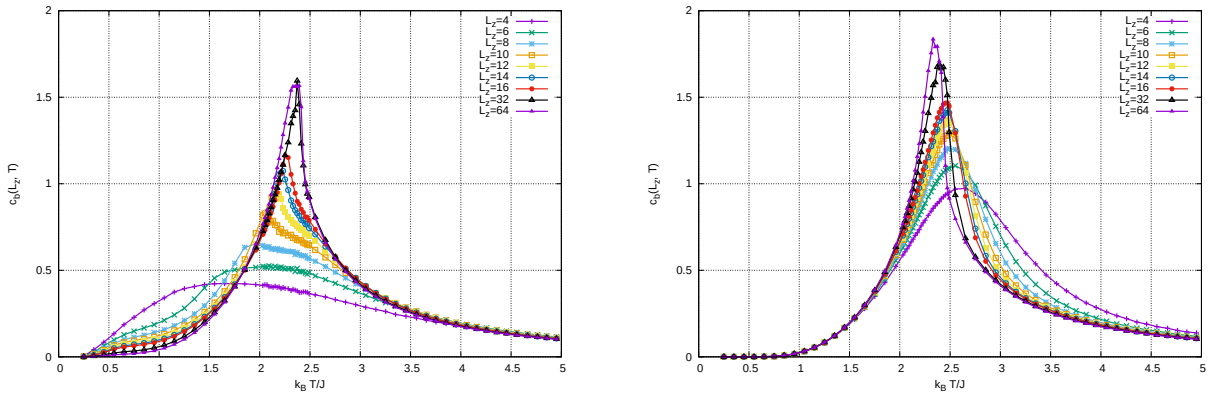

(a) (b)

Figure 4.6: Temperature dependences of $\epsilon_{\rm b}(L_z, T)/\partial T$ with each boundary condition. (a) The anti-parallel boundary. (b) The parallel boundary.

2.40 shows a good agreement with the NEPT point for $v = 10$ with the Metropolis rate in Ref. [24] (see Fig. 2.2). If we assume that the effect of boundary conditions vanishes in the limit of $L_z \to \infty$, we can regard the divergent behavior as the intrinsic NEPT independent of the boundary condition.

We also consider the reason why not only the heat capacity $c(L_z, T)$ but also the temperature derivative of the frictional force density $\partial f(L_z, T)/\partial T$ shows the divergent behavior. The frictional force density $f(L_z, T)$ is estimated by the difference between the expectation value of the energy before the sliding and after over every $1/v$ Monte Carlo sweeps. Then it will be natural to think that both of two kinds of the expectation value have a singularity near $T = 2.40$ and $\partial f(L_z, T)/\partial T$ reflects it.

4.2.4 Checking the Convergence in the Limit $L_x \to \infty$

We now demonstrate that the following two observables are converging in the large size limit.

$$f(L_z, T) := \lim_{L_x \to \infty} \frac{F(L_x, L_z, T)}{L_x}, \tag{4.2}$$

$$\epsilon_{\rm b}(L_z, T) := \lim_{L_x \to \infty} \frac{E_b(L_x.L_z, T)}{L_x L_z}. \tag{4.3}$$

We use the aspect of $L_x = 10L_z, 20L_z, \ldots, 50L_z$ for checking the convergence in the limit $L_x/L_z \to \infty$ with fixed L_z.

Dependence of $F(L_x, L_z, T)/L_x$ on L_x for each L_z

We show that the quantity $F(L_x, L_z, T)/L_x$ has no dependence on L_x for sufficient large size L_x for each size L_z. Figures 4.7, 4.8 show the temperature dependence of the frictional force density under each boundary condition along the z-direction for each of longitudinal size $L_z = 4, 6, 8, 10, 12, 14, 16$ (fig.**??**).

Dependence of $E_{\rm b}(L_x, L_z, T)/(L_x L_z)$ on L_x for each L_z

We show that the quantity $E_{\rm b}(L_x, L_z, T)/L_x$ has no dependence on L_x at a sufficient large L_x for each L_z. The following graphs are the temperature dependence of the frictional force density with each of boundary conditions along the z-direction for each of longitudinal size $L_z = 4, 6, 8, 10, 12, 14, 16$ (fig.**??**).

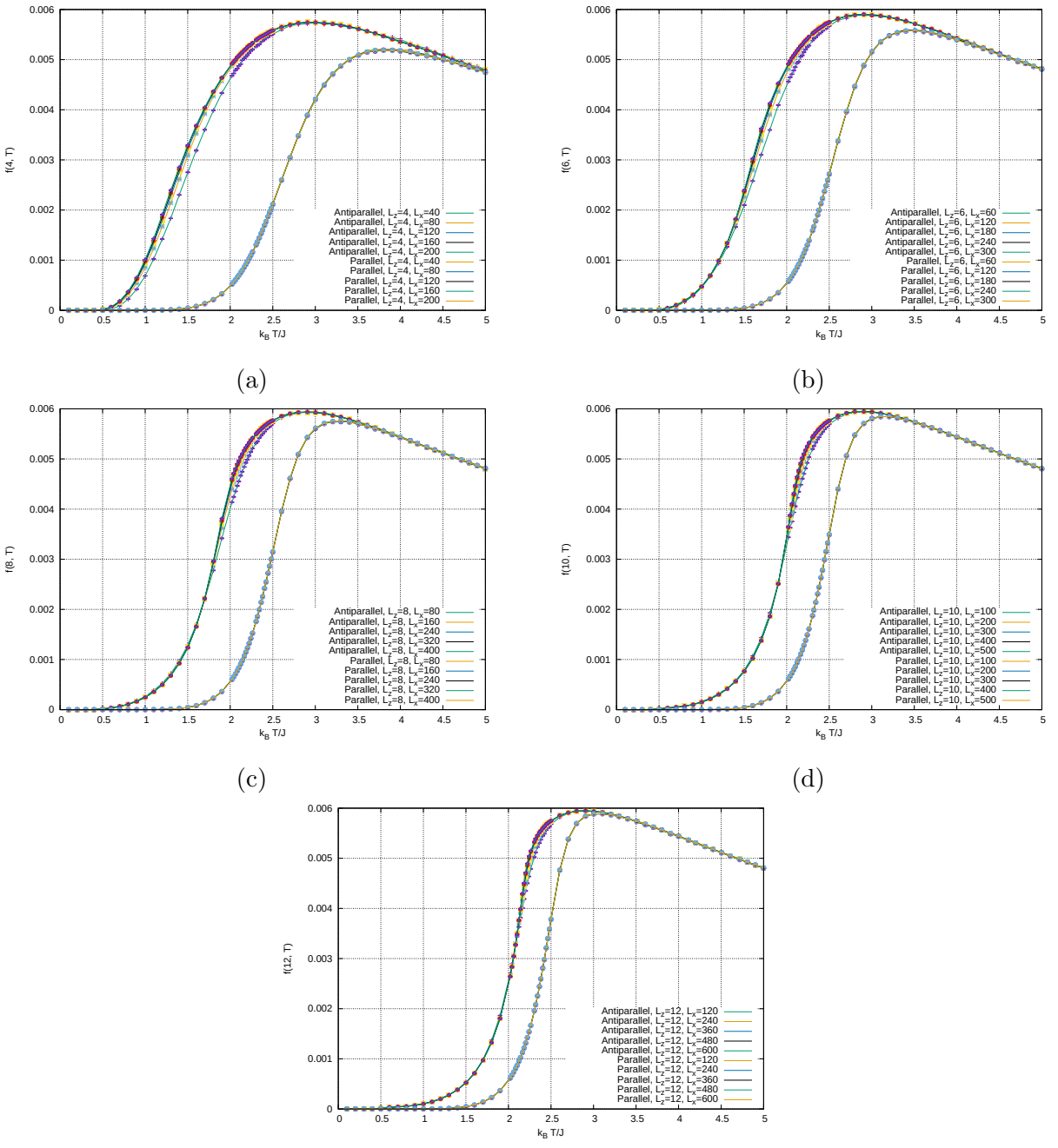

Figure 4.7: Each data shows $F(L_x, L_z, T)/L_x$ versus T. (a) $L_z = 4$. (b) $L_z = 6$. (c) $L_z = 8$. (d) $L_z = 10$. (e) $L_z = 12$.

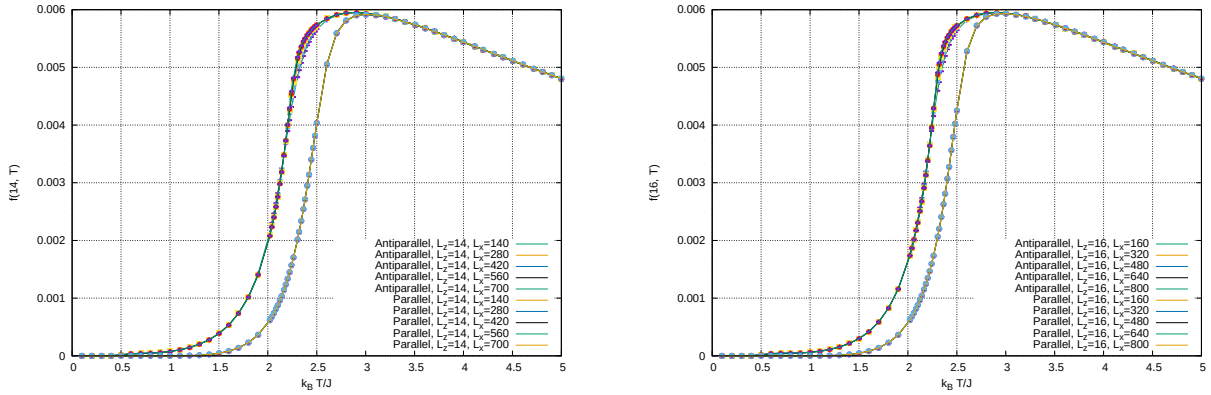

(a)

(b)

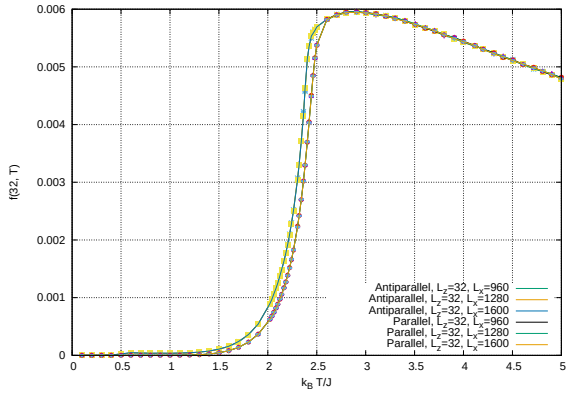

(c)

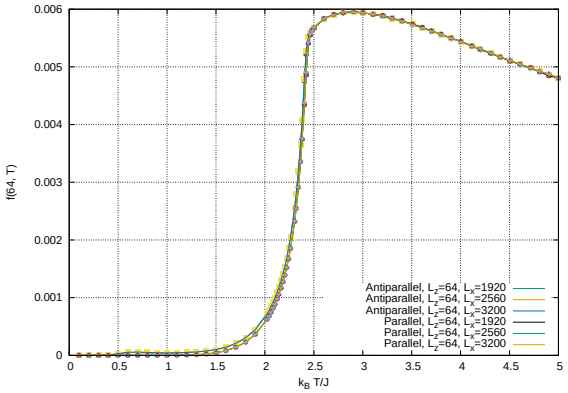

(d)

Figure 4.8: Each data shows $F(L_x, L_z, T)/L_x$ versus T. (a) $L_z = 14$. (b) $L_z = 16$. (c) $L_z = 32$. (d) $L_z = 64$.

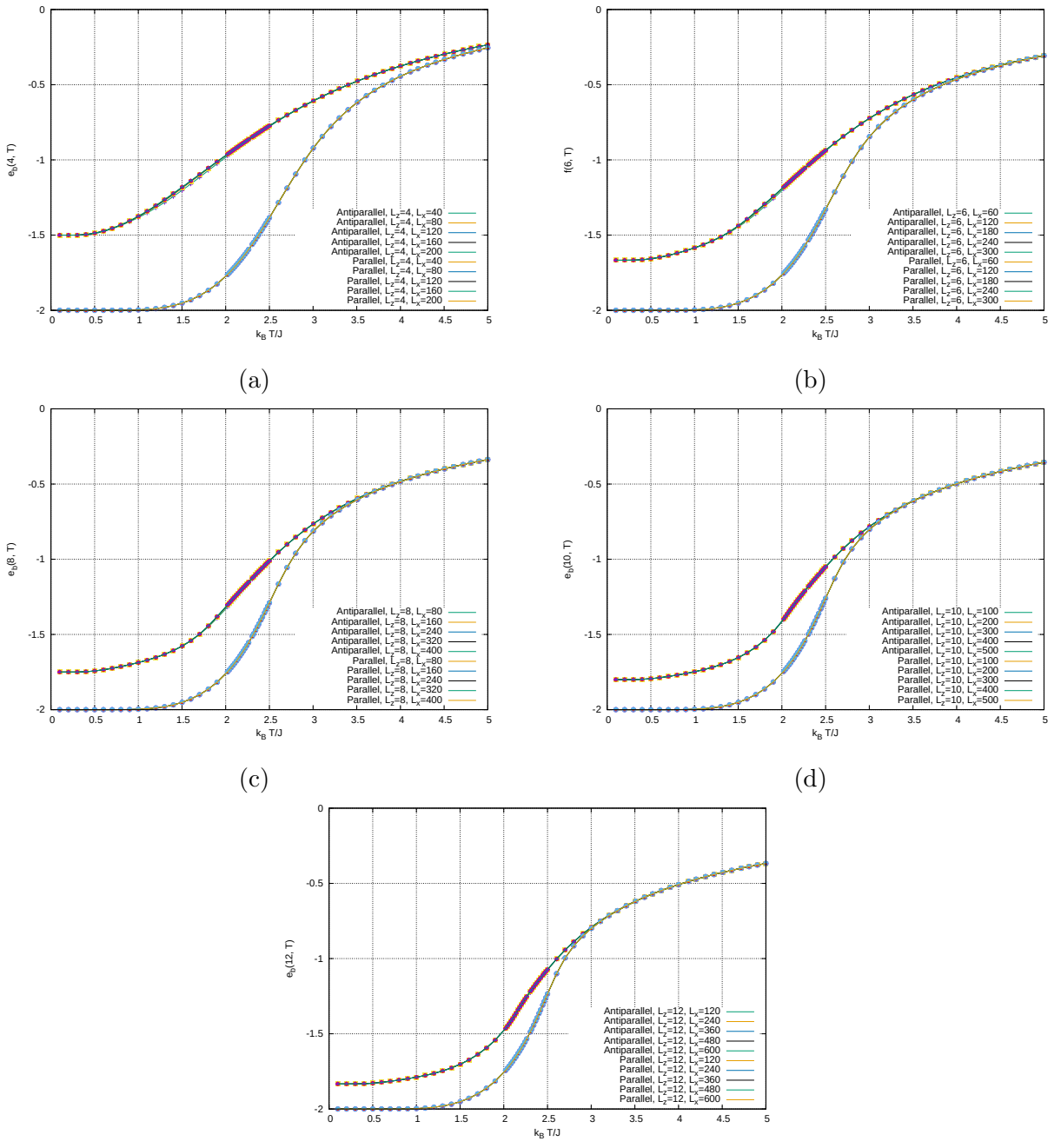

Figure 4.9: Each data shows $E(L_x, L_z, T)/(L_x L_z)$ versus T. (a) $L_z = 4$. (b) $L_z = 6$. (c) $L_z = 8$. (d) $L_z = 10$. (e) $L_z = 12$.

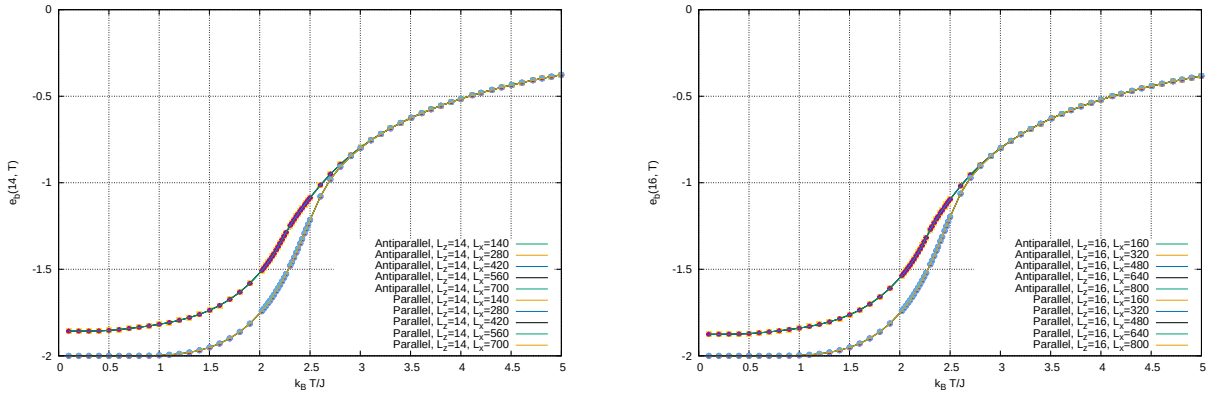

(a)

(b)

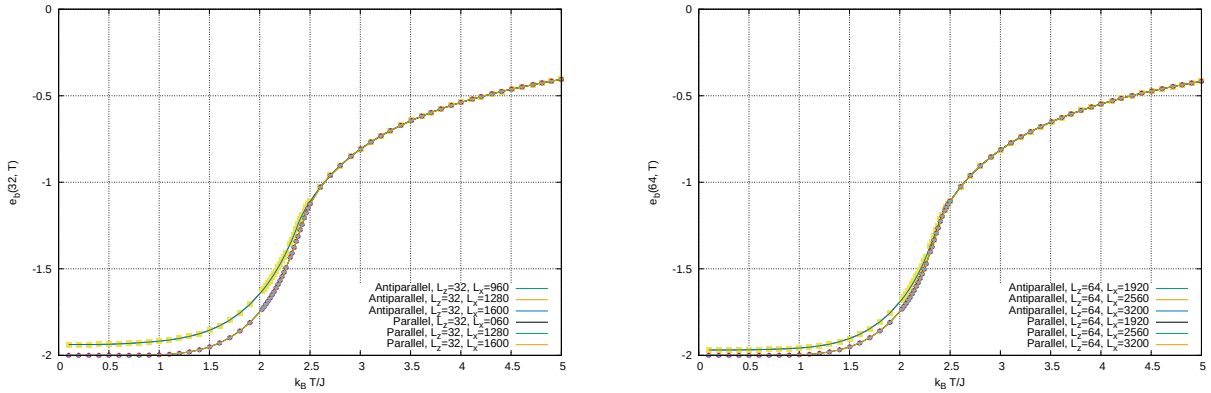

(c)

(d)

Figure 4.10: Each data shows $E(L_x, L_z, T)/(L_x L_z)$ versus T. (a) $L_z = 14$. (b) $L_z = 16$. (c) $L_z = 32$. (d) $L_z = 64$.

Chapter 5

Summary and Discussion

In this research we obtained the result that two different fixed boundary conditions have an effect on the magnetic friction as an effective field: The anti-parallel boundary have a disordering effect and the parallel boundary have a ordering effect. In other words the anti-parallel boundary raises the temperature of the system up and the parallel boundary lowers down. These effects emerge at the sliding boundary when the system behaves as the one-dimension, but vanish when the two-dimension. In addition the crossover between the one-dimension and the two-dimension occurs below the longitudinal size $L_z = 64$ assumed that the transverse size $L_x \to \infty$. Therefore we conclude that we can manipulate the magnetic friction by fixing the boundary condition depending on the temperature when the thickness of the system are enough small.

On the other hand, the efficiency of manipulation is maximized when the system is on, or at least higher than the critical point, thus it is non-trivial that the system has no structural phase transition at such the temperature and that we can consider the magnetic material as an ordinary solid state matter. Therefore, when we consider an experimental setup of the manipulation of the magnetic friction, we also have to take account for the property a the solid

state matter of the magnetic material.

For future works, we are going to investigate

- Consistency between the case of free boundary condition to the results by Hucht[24]
- Divergence of derivatives of the *boundary* energy (or boundary capacity) for the limit of two-dimension
- Behavior of the correlation length itself
- Dimensional crossover of the critical exponents of $\partial f(L_z, T)/\partial T$ and $\partial \epsilon_{\mathrm{b}}/\partial T$

to analyze the phenomena in more detail. We intend to see whether dimensional crossovers in models with other spatial dimensions or continuous symmetries.

Appendix A

Analysis based on Stochastic Matrices

In this chapter, we prove the existence of the non-equilibrium stationary state in our model with a half sliding for arbitrary velocities $v > 0$. In the first section, we discuss the formulation by stochastic matrices, and then see Monte Carlo simulations and the stochastic matrices are equivalent in terms of the probability with a simple example. In the following two sections, we prove several facts for stochastic matrices, which ensures that almost all Monte Carlo simulations converge to a equilibrium state and its uniqueness, and then the properties are taken over and lead to a unique stationary state even if the matrix contains a kind of perturbation factors. In the last two sections, we propose the way to construct the matrix for both equilibrium cases and non-equilibrium stationary cases, and discuss the distributions of their eigenvalues in terms of the convergence.

A.1 A Simple Example: Stochastic Ising Model with N-spins

Monte Carlo simulations for lattice spin systems extract the relevant subspace from the full space instead of an exact calculation of the partition function using a stochastic process. The subspace depends on given parameters and if we use the canonical distribution with a fixed temperature T, the temperature determines the subspace. The stochastic process is expressed as a trajectory of variables by the time in the subspace. Averaging the trajectory for an enough long time, we can compute physical quantities with any desired accuracy.

We now consider a matrix form of the stochastic process. For example, the one-dimensional Ising chain with N-spins has 2^N states. If we labeled each of the states by $i = 1, 2, \ldots, 2^N$, we can write the stochastic time evolution of the system by a set of the existence probabilities $\{p_i(t)\}$ such that the system is in the i-th state at a time t, and the transition probabilities T_{ij} such that the system in the j-th state changes to the i-th state. Note that not the transition probabilities T_{ij} but the existence probabilities $\{p_i(t)\}$ play the role of time evolution.

We additionally define the conditional probability $\tilde{p}_{ij}(t)$ such that the system in the j-th state at a time t changes to the i-th state at the next time $t + 1$. Using the conditional probability, we can derive the relation between the existence probability $p_i(t)$ and the transition probability T_{ij} as

$$\tilde{p}_{ij}(t+1) = T_{ij} p_j(t) \quad \text{for } 1 \leq i, j \leq 2^N. \tag{A.1}$$

From a property as the probability, it should hold that $\sum_{i=1}^{2^N} p_i(t) = 1$ and $p_i(t) \geq 0$ ($i = 1, 2, \ldots, 2^N, t \in \mathbb{R}$). The conditional probability $\tilde{p}_{ij}(t)$ should also satisfy the condition that

$\sum_{j=1}^{2^N} \tilde{p}_{ij}(t) = p_i(t+1)$ $(i = 1, 2, \ldots, 2^N, t \in \mathbb{R})$. Then we have

$$p_i(t+1) = \sum_{j=1}^{2^N} \tilde{p}_{ij}(t+1) = \sum_{j=1}^{2^N} T_{ij} p_j(t) \quad \text{for } 1 \leq i \leq 2^N,\ t \in \mathbb{R}. \tag{A.2}$$

In the other words, the system can be described by the probability vector $\boldsymbol{p}(t) := {}^{\mathrm{t}}(p_1(t), p_2(t), \ldots, p_{2^N}(t))$ and the stochastic matrix $\hat{T} := (T_{ij})$ as

$$\boldsymbol{p}(t+1) = \hat{T}\boldsymbol{p}(t) \quad \text{for } t \in \mathbb{R}. \tag{A.3}$$

In Monte Carlo simulations, we often trace the trajectory of a component of the vector $\boldsymbol{p}(t)$, thus we rarely need to construct the matrix $\hat{T}$. But it is helpful for us to consider such the matrix when we discuss the convergence to the stationary state or its uniqueness. These discussions are valid for general Ω-dimensional state spaces, thus we denote the number of states by Ω from now on.

A.2 General Theory of Stochastic Matrices

In this section we discuss the conditions which ensure a convergence of the corresponding Monte Carlo simulation to a unique stationary state. We first define the stochastic matrix and discuss fundamental properties of the stochastic matrix. We next discuss the properties which result from an additional condition called *weak/strong connectivity*, which leads the existence and the uniqueness of a stationary state. We also see that we can construct a stochastic matrix which leads to any desired stationary state under the so-called *detailed balanced condition*.

From the condition $\sum_{i=1}^{\Omega} p_i(t) = 1$ and $p_i(t) \geq 0$ $(i = 1, 2, \ldots, \Omega, t \in \mathbb{R})$, we have a set of properties $\sum_{i=1}^{\Omega} T_{ij} = 1$, $T_{ij} \geq 0$ $(1 \leq i \leq \Omega)$. Any matrix with these conditions is called

stochastic matrix and shows the following interesting property:

Theorem A.2.1. Let $\hat{T}$ be a stochastic matrix, then all absolute values of eigenvalue are less than or equal to 1. For any eigenvector $\boldsymbol{x} = {}^{\mathrm{t}}\{x_1, x_2, \ldots, x_\Omega\}$ which does *not* belong to the eigenvalue 1, it additionally holds that

$$\sum_{i=1}^{\Omega} x_j = 0. \tag{A.4}$$

We now define the vector $\boldsymbol{d} := {}^{\mathrm{t}}(1, 1, \ldots, 1)$ to prove all facts after this.

Proof. For any stochastic matrix $\hat{T}$, we have

$$\left({}^{\mathrm{t}}\hat{T}\boldsymbol{d}\right)_i = \sum_{j=1}^{\Omega} \left({}^{t}T\right)_{ij} d_j = \sum_{j=1}^{\Omega} T_{ji} d_j = \sum_{j=1}^{\Omega} T_{ji} = 1 \quad \text{for } i = 1, 2, \ldots, \Omega, \tag{A.5}$$

$$\iff \quad {}^{\mathrm{t}}\hat{T}\boldsymbol{d} = \boldsymbol{d}. \tag{A.6}$$

Therefore the matrix ${}^{\mathrm{t}}\hat{T}$ has an eigenvalue 1 at least. The eigenequation for the matrix ${}^{\mathrm{t}}\hat{T}$ are rewritten as

$$\det\left[\lambda\hat{I}_\Omega - {}^{\mathrm{t}}\hat{T}\right] = \det\left[{}^{\mathrm{t}}\left(\lambda\hat{I}_\Omega - \hat{T}\right)\right] = \det\left[\lambda\hat{I}_\Omega - \hat{T}\right], \tag{A.7}$$

and then the set of eigenvalues of $\hat{T}$ is equal to that of ${}^{\mathrm{t}}\hat{T}$. Finally the matrix $\hat{T}$ has an eigenvalue 1 at least. A general eigenvalue equation of $\hat{T}$ can be written as

$$\hat{T}\boldsymbol{x}_\lambda = \lambda\boldsymbol{x}_\lambda, \tag{A.8}$$

where $\boldsymbol{x}_\lambda = {}^{\mathrm{t}}(x_{\lambda,1}, x_{\lambda,2}, \ldots, x_{\lambda,\Omega})$ is its eigenvector. We have

$$((l.h.s \text{ of A.8}), \boldsymbol{d}) = (\hat{T}\boldsymbol{x}_\lambda, \boldsymbol{d}) = (\boldsymbol{x}_\lambda, {}^{\mathrm{t}}\hat{T}\boldsymbol{d}) = (\boldsymbol{x}_\lambda, \boldsymbol{d}), \tag{A.9}$$

$$((r.h.s \text{ of A.8}), \boldsymbol{d}) = (\lambda\boldsymbol{x}_\lambda, \boldsymbol{d}) = \lambda(\boldsymbol{x}_\lambda, \boldsymbol{d}). \tag{A.10}$$

$$\iff \quad (1-\lambda)(\boldsymbol{x}_\lambda, \boldsymbol{d}) = 0 \quad \iff \quad \lambda = 1 \text{ or } (\boldsymbol{x}_\lambda, \boldsymbol{d}) = 0. \tag{A.11}$$

$$\iff \quad \sum_{i=1}^{\Omega} x_{\lambda,i} = 0 \quad \text{if } \lambda \neq 1. \tag{A.12}$$

We additionally define the vector $\boldsymbol{y}_\lambda := {}^{\mathrm{t}}(|x_{\lambda,1}|, |x_{\lambda,2}|, \ldots, |x_{\lambda,\Omega}|)$ for any λ. From the equation $\sum_{j=1}^{\Omega} T_{ij}x_{\lambda,j} = \lambda x_i (i = 1, 2, \ldots, \Omega)$ we have

$$|\sum_{j=1}^{\Omega} T_{ij}x_{\lambda,j}| \leq \sum_{j=1}^{\Omega} T_{ij}|x_{\lambda,j}| \quad (\because T_{ij} \geq 0 \quad \text{for } j = 1, 2, \ldots, \Omega) \tag{A.13}$$

$$= \left(\hat{T}\boldsymbol{y}_\lambda\right)_i \quad \text{for } i = 1, 2, \ldots, \Omega. \tag{A.14}$$

and the left hand side of (A.14) are rewritten as

$$|\sum_{j=1}^{\Omega} T_{ij}x_{\lambda,j}| = |\lambda x_{\lambda,j}| = |\lambda| \times |x_{\lambda,j}| = |\lambda| \times (\boldsymbol{y}_\lambda)_j\,, \tag{A.15}$$

thus we have

$$|\lambda| \times (\boldsymbol{y}_\lambda)_j \leq \left(\hat{T}\boldsymbol{y}_\lambda\right)_i\,, \tag{A.16}$$

$$\iff \quad |\lambda| \times (\boldsymbol{y}_\lambda, \boldsymbol{d}) \leq \left(\hat{T}\boldsymbol{y}_\lambda, \boldsymbol{d}\right) = \left(\boldsymbol{y}_\lambda, {}^{\mathrm{t}}\hat{T}\boldsymbol{d}\right) = (\boldsymbol{y}_\lambda, \boldsymbol{d})\,, \tag{A.17}$$

$$\iff \quad |\lambda| \leq 1. \tag{A.18}$$

□

We limit the class of stochastic matrices to that of weakly connected ones from now on.

Definition A.2.1. For an arbitrary $1 \leq i, j \leq \Omega$, if there exists an $n(i,j) > 0$ such that

$$\left(\hat{T}^{n(i,j)}\right)_{ij} > 0, \tag{A.19}$$

the matrix $\hat{T}$ is called *weakly connected*. Note that for any $n' > n(i,j)$ it does *not* follows that $\left(\hat{T}^{n'}\right) > 0$.

To make proofs easier, we also define the matrix $\hat{\mathcal{T}}_\epsilon$ ($\epsilon > 0$) and discuss its properties. Denoting the maximum value of $n(i,j)$ by $n_{\max} := \max_{1 \leq i,j \leq \Omega} [n(i,j)]$ and defining the matrix $\hat{\mathcal{T}}_\epsilon := \left(\hat{I}_\Omega + \epsilon \hat{T}\right)^{n_{\max}}$, we have

$$\left(\hat{\mathcal{T}}_\epsilon\right)_{ij} = \left(\left(\hat{I}_\Omega + \epsilon \hat{T}\right)^{n_{\max}}\right)_{ij} = \sum_{k=1}^{n_{\max}} \binom{n_{\max}}{k} \left(\hat{I}_\Omega^k \left(\epsilon \hat{T}\right)^{n_{\max}-k}\right)_{ij} \tag{A.20}$$

$$= \sum_{k=1}^{n_{\max}} \binom{n_{\max}}{k} \epsilon^{n_{\max}-k} \left(\hat{T}^{n_{\max}-k}\right)_{ij} \geq 0 \quad (\because T_{ij} > 0) \quad \text{for } 1 \leq i, j \leq \Omega. \tag{A.21}$$

For the eigenvector $\boldsymbol{x}_1 = {}^{\mathrm{t}}(x_{1,1}, x_{1,2}, \ldots, x_{1,\Omega})$, which belongs to the eigenvalue 1, it holds that

$$\hat{\mathcal{T}}_\epsilon \boldsymbol{x}_1 = \sum_{k=1}^{n_{\max}} \binom{k}{n_{\max}} \epsilon^{n_{\max}-k} \hat{T}^{n_{\max}} \boldsymbol{x}_1 \tag{A.22}$$

$$= \sum_{k=1}^{n_{\max}} \binom{k}{n_{\max}} \epsilon^{n_{\max}-k} \boldsymbol{x}_1 \tag{A.23}$$

$$= (1+\epsilon)^{n_{\max}} \boldsymbol{x}_1, \tag{A.24}$$

and each component is

$$\sum_{j=1}^{\Omega} \left(\hat{\mathcal{T}}_\epsilon\right)_{ij} x_{1,j} = (1+\epsilon)^{n_{\max}} x_{1,i} \quad \text{for } i = 1, 2, \ldots, \Omega. \tag{A.25}$$

Theorem A.2.2. The phases of components of the vector $\boldsymbol{x}_1$ are aligned together and all the components are positive. In other words, we can decompose the vector into a phase factor and a positive vector as follows

$$\boldsymbol{x}_1 = \mathrm{e}^{i\theta} \boldsymbol{u}_1, \tag{A.26}$$

where θ is the phase and $\boldsymbol{u}_1$ is the vector with all positive component.

Proof. If components of the vector $\boldsymbol{x}_1$ are *not* aligned together such that $\sum_{i=1}^{\Omega} |x_{1,i}| > |\sum_{i=1}^{\Omega} x_{1,i}|$ holds, we have

$$|\sum_{j=1}^{\Omega} \left(\hat{\mathcal{T}}_\epsilon\right)_{ij} x_{1,j}| < \sum_{j=1}^{\Omega} \left(\hat{\mathcal{T}}_\epsilon\right)_{ij} |x_{1,j}| = (1+\epsilon)^{n_{\max}} |x_{1,i}|. \tag{A.27}$$

On the other hand, the row-wise sum of the matrix $\hat{\mathcal{T}}_\epsilon$ are

$$\sum_{i=1}^{\Omega} \left(\hat{\mathcal{T}}_\epsilon\right)_{ij} = \sum_{k=1}^{n_{\max}} \binom{k}{n_{\max}} \epsilon^{n_{\max}-k} \sum_{i=1}^{\Omega} \left(\hat{T}^{n_{\max}-k}\right)_{ij} = (1+\epsilon)^{n_{\max}}. \tag{A.28}$$

Then we have

$$\sum_{i=1}^{\Omega}\sum_{j=1}^{\Omega} \left(\hat{\mathcal{T}}_\epsilon\right)_{ij} |x_{1,j}| = (1+\epsilon)^{n_{\max}} \sum_{j=1}^{\Omega} |x_{1,j}| > (1+\epsilon)^{n_{\max}} \sum_{i=1}^{\Omega} |x_{1,i}|, \tag{A.29}$$

but it is the contradiction caused from our assumption $\sum_{i=1}^{\Omega} |x_{1,i}| > |\sum_{i=1}^{\Omega} x_{1,i}|$. Furthermore the left hand side of (A.25) is positive because that $n_{\max}$ is the maximum value of $n(i,j)$, and

then the right hand side is also positive. Then we have $x_{1,i} > 0 (i = 1, 2, \ldots, \Omega)$. □

Theorem A.2.3. The eigenspace of the matrix $\hat{\mathcal{T}}_\epsilon$, which belongs to the eigenvalue 1, is *one-dimensional*.

Proof. If we have two different eigenvectors, which belongs to the eigenvalue 1, we can write their eigenequations by two different *positive vectors* as

$$\hat{T}\boldsymbol{u}_1 = \boldsymbol{u}_1, \tag{A.30}$$

$$\hat{T}\boldsymbol{v}_1 = \boldsymbol{v}_1. \tag{A.31}$$

For their any linear superposition, we also have

$$\hat{T}(\boldsymbol{u}_1 + tv_1) = \boldsymbol{u}_1 + tv_1, \quad \text{for any } t \in \mathbb{R}. \tag{A.32}$$

But if two eigenvectors $\boldsymbol{u}_1$ and $\boldsymbol{v}_1$ are not aligned, we can make a non-trivial vector with a certain t such that $(\boldsymbol{u}_1 + tv_1)_l = 0$ for an l-th element. But it is the contradiction with the fact $x_{1,i} > 0 (i = 1, 2, \ldots, \Omega)$. Then we have no eigenspaces more than one, which belongs to the eigenvalue 1. □

We additionally limit the class of stochastic matrices to that of strongly connected ones from now on.

Definition A.2.2. If there exists a number $N_0 > 0$ such that

$$\left(\hat{T}^{N_0}\right)_{ij} > 0 \tag{A.33}$$

for an arbitrary $1 \leq i, j \leq \Omega$, the matrix $\hat{T}$ is called *strongly connected*.

Theorem A.2.4. There exists only the eigenvalue 1 with its absolute value 1.

Proof. We now have $\hat{T}^n \boldsymbol{u}_\lambda = \lambda^n \boldsymbol{u}_\lambda$, where $\boldsymbol{u}_\lambda = {}^{\mathrm{t}}(u_{\lambda,1}, u_{\lambda,2}, \ldots, u_{\lambda,\Omega})$ is the eigenvector which belongs to an eigenvalue λ. Their components are written as

$$\sum_{j=1}^{\Omega} \left(\hat{T}^n\right)_{ij} u_{\lambda,j} = \lambda^n \boldsymbol{u}_{\lambda,i}, \quad \text{for } i = 1, 2, \ldots, \Omega. \tag{A.34}$$

We can divide conditions for λ into following two cases:

Case1: $\sum_{i=1}^{\Omega} |u_{\lambda,i}| > |\sum_{i=1}^{\Omega} u_{\lambda,i}|$**,**

We have

$$\sum_{j=1}^{\Omega} \left(\hat{T}^n\right)_{ij} |u_{\lambda,j}| > |\sum_{j=1}^{\Omega} \left(\hat{T}^n\right)_{ij} u_{\lambda,j}| = |\lambda^n| \times |u_{\lambda,i}|, \quad \text{for } i = 1, 2, \ldots, \Omega. \tag{A.35}$$

$$\iff \quad |\lambda^n| < 1 \quad \iff \quad |\lambda| < 1. \tag{A.36}$$

Case2: $\sum_{i=1}^{\Omega} |u_{\lambda,i}| = |\sum_{i=1}^{\Omega} u_{\lambda,i}|$**.**

We have

$$\sum_{i=1}^{\Omega} \sum_{j=1}^{\Omega} \left(\hat{T}^n\right)_{ij} u_{\lambda,j} = \sum_{j=1}^{\Omega} u_{\lambda,j} = \lambda^n \sum_{i=1} u_{\lambda,i}. \tag{A.37}$$

$$\iff \quad \lambda^n = 1 \quad (\because \boldsymbol{u}_\lambda \neq \boldsymbol{0}, u_{\lambda,i} \geq 0 \Rightarrow \sum_{i=1}^{\Omega} u_{\lambda,i} > 0). \tag{A.38}$$

Thus there is only an eigenvalue 1 with its absolute value 1. □

Theorem A.2.5. The vector $\lim_{N\to\infty} \hat{T}^N \boldsymbol{r} = \boldsymbol{0}$ for any $\boldsymbol{r} \in \mathbb{C}$ is orthogonal to $\boldsymbol{d}$.

Proof. For an arbitrary vector $\boldsymbol{r}$, we can decompose it into its real and imaginary parts as

$\boldsymbol{r} = \boldsymbol{r}_{\mathrm{R}} + i\boldsymbol{r}_{\mathrm{I}}$. Since the condition $(\boldsymbol{r}, \boldsymbol{d}) = 0$ is equivalent to $\sum_{i=1}^{\Omega} r_i = 0$, we have

$$\sum_{j \in I_+} r_j + \sum_{j \in I_-} r_j = 0, \tag{A.39}$$

where $I_\pm := \{j \mid r_j \gtrless 0, 1 \leq j \leq \Omega\}$. Note that $\sum_{j \in I_+} r_j = \sum_{j \in I_-} |r_j|$. Thus we have

$$\sum_{j \in I_+} r_j = \sum_{j \in I_-} |r_j| = \|\boldsymbol{r}\|_1 / 2. \tag{A.40}$$

Since $\hat{T}$ is strongly connected, there is an integer N_0 such that $\left(\hat{T}^{N_0}\right)_{ij} > 0$ for an arbitrary $1 \leq i, j \leq \Omega$. For the N_0 we have

$$\left(\hat{T}^{N_0}\boldsymbol{r}\right) = \sum_{j=1}^{\Omega} \left(\hat{T}^{N_0}\right)_{ij} r_j = \sum_{j \in I_+} \left(\hat{T}^{N_0}\right)_{ij} r_j - \sum_{j \in I_-} \left(\hat{T}^{N_0}\right)_{ij} |r_j| \tag{A.41}$$

$$= \sum_{j=1}^{\Omega} \left(\hat{T}^{N_0}\right)_{ij} r_j - 2 \sum_{j \in I_-} \left(\hat{T}^{N_0}\right)_{ij} |r_j| \tag{A.42}$$

$$\leq \sum_{j=1}^{\Omega} \left(\hat{T}^{N_0}\right)_{ij} r_j - 2\delta_{N_0} \sum_{j \in I_-} |r_j| \tag{A.43}$$

$$= \sum_{j=1}^{\Omega} \left(\hat{T}^{N_0}\right)_{ij} r_j - \delta_{N_0} \|\boldsymbol{r}\|_1, \tag{A.44}$$

where $\delta_{N_0} := \min_{1 \leq i,j \leq \Omega} \left[\left(\hat{T}^{N_0}\right)_{ij}\right]$ (for $i = 1, 2, \ldots, \Omega$). Note that there exists a $\delta_{N_0} > 0$ for the

strongly connected matrix $\hat{T}$. Similarly we have

$$\left(\hat{T}^{N_0}\boldsymbol{r}\right) = \sum_{j=1}^{\Omega}\left(\hat{T}^{N_0}\right)_{ij} r_j = \sum_{j\in I_+}\left(\hat{T}^{N_0}\right)_{ij} r_j - \sum_{j\in I_-}\left(\hat{T}^{N_0}\right)_{ij} |r_j| \tag{A.45}$$

$$=2\sum_{j\in I_+}\left(\hat{T}^{N_0}\right)_{ij} r_j - \sum_{j=1}^{\Omega}\left(\hat{T}^{N_0}\right)_{ij} |r_j| \tag{A.46}$$

$$\geq 2\delta_{N_0}\sum_{j\in I_+} r_j - \sum_{j=1}^{\Omega}\left(\hat{T}^{N_0}\right)_{ij} |r_j| \tag{A.47}$$

$$=\delta_{N_0}\|\boldsymbol{r}\|_1 - \sum_{j=1}^{\Omega}\left(\hat{T}^{N_0}\right)_{ij} |r_j|, \quad (\text{for } i = 1, 2, \ldots, \Omega). \tag{A.48}$$

Combining them, we have

$$|\left(\hat{T}^{N_0}\boldsymbol{r}\right)| \leq \sum_{j=1}^{\Omega}\left(\hat{T}^{N_0}\right)_{ij} |r_j| - \delta_{N_0}\|\boldsymbol{r}\|_1, \quad (\text{for } i = 1, 2, \ldots, \Omega), \tag{A.49}$$

and then it holds that

$$\|\hat{T}^{N_0}\boldsymbol{r}\|_1 = \sum_{i=1}^{\Omega}|\left(\hat{T}^{N_0}\boldsymbol{r}\right)_i| \leq \sum_{j=1}^{\Omega}|r_j| - N_0\delta_{N_0}\|\boldsymbol{r}\|_1 = (1 - N\delta_{N_0})\|\boldsymbol{r}\|_1. \tag{A.50}$$

The vector $\hat{T}^{N_0}\boldsymbol{r}$ is also orthogonal to the vector $\boldsymbol{d}$, actually it holds that

$$\left(\hat{T}^{N_0}\boldsymbol{r}, \boldsymbol{d}\right) = \left(\boldsymbol{r}, {}^{\mathrm{t}}\left(\hat{T}^{N_0}\right)\boldsymbol{d}\right) = \left(\boldsymbol{r}, \left({}^{\mathrm{t}}\hat{T}\right)^{N_0}\boldsymbol{d}\right) = (\boldsymbol{r}, \boldsymbol{d}) = 0. \tag{A.51}$$

Then, for any positive integer l, we can repeat this discussion as

$$\|\hat{T}^{N_0 l}\boldsymbol{r}\|_1 \leq (1 - N_0\delta_{N_0})^l\|\boldsymbol{r}\|_1. \tag{A.52}$$

Since $N_0 > 0, \delta_{N_0} > 0$ and thus $1 - N_0\delta_{N_0} < 0$, we have

$$\lim_{l\to\infty}(1 - N_0\delta_{N_0})^l \|\boldsymbol{r}\|_1 = 0. \tag{A.53}$$

$$\iff \quad \lim_{l\to\infty} \|\hat{T}^{N_0 l}\boldsymbol{r}\|_1 = 0. \tag{A.54}$$

Thus, for an arbitrary positive integer N, we have

$$\lim_{N\to\infty} \|\hat{T}^N \boldsymbol{r}\|_1 = 0. \tag{A.55}$$

□

Theorem A.2.6. We can write any vector $\boldsymbol{x}$ as the superposition of $\boldsymbol{u}_1$ and $\boldsymbol{r}$.

Proof. Defining the coefficient $c_{1,\boldsymbol{x}} := (\boldsymbol{x}, \boldsymbol{d})/(\boldsymbol{u}_1, \boldsymbol{d})$ and the vector $\boldsymbol{r}_{\boldsymbol{x}} := \boldsymbol{x} - c_{1,\boldsymbol{x}}\boldsymbol{u}_1$, we have

$$(\boldsymbol{r}_{\boldsymbol{x}}, \boldsymbol{d}) = (\boldsymbol{x}, \boldsymbol{d}) - \frac{(\boldsymbol{x}, \boldsymbol{d})}{(\boldsymbol{u}_1, \boldsymbol{d})}(\boldsymbol{u}_1, \boldsymbol{d}) = 0, \tag{A.56}$$

$$\boldsymbol{x} = c_{1,\boldsymbol{x}}(\boldsymbol{u}_1, \boldsymbol{d}) + \boldsymbol{r}_{\boldsymbol{x}}. \tag{A.57}$$

□

Theorem A.2.7. The limit $\lim_{N\to\infty} \hat{T}^N \boldsymbol{p}^{(0)}$ is independent on the initial vector $\boldsymbol{p}^{(0)}$ and it holds that

$$\lim_{N\to\infty} \hat{T}^N \boldsymbol{p}^{(0)} = \frac{\boldsymbol{u}_1}{\|\boldsymbol{u}_1\|_1}, \tag{A.58}$$

where the vector $\boldsymbol{p}^{(0)} = {}^{\mathrm{t}}\left\{p_1^{(0)}, p_2^{(0)}, \ldots, p_\Omega^{(0)}\right\}$ is in the class of probability vectors and then it is normalized $\sum_{i=1}^{\Omega} p_i^{(0)} = 1$.

Proof. From the theorem A.2.6, we have

$$\hat{T}^N \boldsymbol{p}^{(0)} = c_{1,\boldsymbol{p}^{(0)}} \hat{T}^N \boldsymbol{u}_1 + \hat{T}^N \boldsymbol{r}_{\boldsymbol{p}^{(0)}} = c_{1,\boldsymbol{p}^{(0)}} \boldsymbol{u}_1 + \hat{T}^N \boldsymbol{r}_{\boldsymbol{p}^{(0)}}. \tag{A.59}$$

Its limit $N \to \infty$ is taken as

$$\lim_{N\to\infty} \hat{T}^N \boldsymbol{p}^{(0)} = c_{1,\boldsymbol{p}^{(0)}} \boldsymbol{u}_1 + \lim_{N\to\infty} \hat{T}^N \boldsymbol{r}_{\boldsymbol{p}^{(0)}} = c_{1,\boldsymbol{p}^{(0)}} \boldsymbol{u}_1. \tag{A.60}$$

Using the matrix $\hat{A} := {\boldsymbol{u}_1}^{\mathrm{t}} \boldsymbol{d} / (\boldsymbol{u}_1, \boldsymbol{d})$, we have

$$\left(\hat{A}\boldsymbol{p}^{(0)}\right)_i = \sum_{j=1}^{\Omega} \frac{(\boldsymbol{u}_1)_i}{(\boldsymbol{u}_1, \boldsymbol{d})} \left(\boldsymbol{p}^{(0)}\right)_j = \left(\boldsymbol{p}^{(0)}, \boldsymbol{d}\right) \frac{(\boldsymbol{u}_1)_i}{(\boldsymbol{u}_1, \boldsymbol{d})}, \quad \text{for } i = 1, 2, \ldots, \Omega. \tag{A.61}$$

Then it leads

$$\hat{A}\boldsymbol{p}^{(0)} = \frac{(\boldsymbol{u}_1)_i}{(\boldsymbol{u}_1, \boldsymbol{d})} \boldsymbol{p}^{(0)} = c_{1,\boldsymbol{p}^{(0)}} \boldsymbol{p}^{(0)}. \tag{A.62}$$

Then the limit $N \to \infty$ for $\hat{T}^N \boldsymbol{p}^{(0)}$ is rewritten by a simple multiplication as follows

$$\lim_{N\to\infty} \hat{T}^N \boldsymbol{p}^{(0)} = \frac{{\boldsymbol{u}_1}^{\mathrm{t}} \boldsymbol{d}}{(\boldsymbol{u}_1, \boldsymbol{d})} \boldsymbol{p}^{(0)}. \tag{A.63}$$

The expression (A.63) lead to the relation $\lim_{N\to\infty} \hat{T}^N \boldsymbol{p}^{(0)} = \boldsymbol{u}_1 / \|\boldsymbol{u}_1\|_1$. Actually it holds that

$$\frac{{\boldsymbol{u}_1}^{\mathrm{t}} \boldsymbol{d}}{(\boldsymbol{u}_1, \boldsymbol{d})} \left(\boldsymbol{p}^{(0)}\right)_i = \frac{\sum_{j=1}^{\Omega} (\boldsymbol{u}_1)_i (\boldsymbol{d})_j \left(\boldsymbol{p}^{(0)}\right)_j}{(\boldsymbol{u}_1, \boldsymbol{d})} = \frac{u_{1,i}}{\|\boldsymbol{u}_1\|_1}, \tag{A.64}$$

thus we have

$$\lim_{N\to\infty} \hat{T}^N \boldsymbol{p}^{(0)} = \frac{\boldsymbol{u}_1}{\|\boldsymbol{u}_1\|_1}. \tag{A.65}$$

□

Once we get a strongly connected stochastic matrix $\hat{T}$, its stationary distribution $\boldsymbol{u}_1/\|\boldsymbol{u}_1\|_1$ is determined independently on the initial distribution. We can consider this procedure as a *transformation* from the matrix $\hat{T}$ into the vector $\boldsymbol{u}_1/\|\boldsymbol{u}_1\|_1$.

A.3 Construction of the Stochastic Matrix based on the Detailed Balanced Condition

On the other hand, we can also consider the inverse transformation. This means the *construction* of the matrix $\hat{T}'$ with a *desired* stationary distribution $\boldsymbol{p}'$. We can actually formulate such the procedure using the *detailed balanced condition* as follows.

Definition A.3.1. If a vector $\boldsymbol{p}' = {}^{\mathrm{t}}(p'_1, p'_2, \ldots, p'_\Omega)$ is the stationary distribution of the stochastic matrix $\hat{T}' = \left(T'_{ij}\right)$, it holds that

$$T'_{ij}p'_j = T'_{ji}p'_i \tag{A.66}$$

for $1 \leq i, j \leq \Omega$.

This property is simplified by summing over the subscription i as follows

$$\sum_{i=1}^{\Omega} T'_{ij}p'_j = p'_j = \sum_{i=1}^{\Omega} T'_{ji}p'_i = \left(\hat{T}\boldsymbol{p}'\right)_j, \quad \text{for } j = 1, 2, \ldots, \Omega. \tag{A.67}$$

Then if the detailed balanced condition holds for a matrix $\hat{T}'$, the corresponding vector $\boldsymbol{p}'$ is the fixed point of the matrix $\hat{T}'$. Thus in order to get the matrix $\hat{T}'$ which lead any distribution $\boldsymbol{p}^{(0)}$ to the desired distribution $\boldsymbol{p}'$, we only have to construct each element T'_{ij} of the matrix according to the condition (A.66) and make the matrix strongly connected.

In Monte Carlo simulations of statistical mechanics, we calculate the equilibrium distribution $\boldsymbol{p}_{\rm eq}(\beta)$ at an inverse temperature β using an initial state i_0 and a rule of the stochastic process $i \to j \to j' \to \ldots$. We can regard the matrix construction method as a set of the stochastic process $i_0 \to j \to j' \to \ldots$ over all possible states $i_0 = 1, 2, \ldots, \Omega$. In other words, the matrix T_{ij} corresponding to a simulation contains the information of all possible initial states $i_0 = 1, 2, \ldots, \Omega$ and all possible transitions $T_{1,i_0}, T_{2,i_0}, \ldots, T_{\Omega,i_0}$ respectively from them. Thus we often consider a *sample path* by an appropriate initial state and the matrix.

The condition (A.66) or

$$\frac{T_{ij}}{T_{ji}} = \frac{p_i}{p_j} \tag{A.68}$$

is not sufficient to determine a concrete form of the matrix $\hat{T}$ and thus in general there is a degree of freedom in the form of $\hat{T}$. For Monte Carlo simulations of equilibrium statistical mechanics, this freedom also remains as follows:

$$\frac{T_{ij}(\beta)}{T_{ji}(\beta)} = \frac{p_i(\beta)}{p_j(\beta)} = \mathrm{e}^{-\beta(E_i - E_j)}, \quad \text{for } 1 \le i, j \le \Omega, \tag{A.69}$$

where $T_{ij}(\beta)$ and $p_i(\beta)$ are the matrix corresponding to a simulation and the probability that the i-th state emerges respectively with a fixed inverse temperature β. But this relation is important that the rate of transition probabilities is always given by a difference of energy eigenvalues $\{E_1, E_2, \ldots, E_\Omega\}$, and thus we do *not* have to calculate exact values of $\tilde{p}_i(\beta) :=$

$\exp[-\beta E_i]/Z(\beta)$ ($Z(\beta) := \sum_i \exp[-\beta E_i]$).

If we use the Metropolis probability for the N-spins system, each element of the matrix $(T_{ij}(\beta))$ is written as follows.

$$T_{ij}(\beta) = \begin{cases} \frac{1}{N}\min\left[1, \mathrm{e}^{-\beta(E_i - E_j)}\right] & \text{for states } i,j \text{ mutually reacheable by a single flip,} \\ 0 & \text{for states } i,j \textit{ not} \text{ mutually reacheable by a single flip.} \end{cases} \tag{A.70}$$

The factor $1/N$ describes the equivalent selection of a spin to flip.

We call the matrix with the condition (A.70) *Metropolis matrix* and denote by $(M_{ij}) := (T_{ij}(\beta))\,|_{(\text{A.70})}$ from now on.

Metropolis matrices generally have few non-zero elements due to not taking transitions between all energy eigenstates into account. Thus the Monte Carlo simulation with Metropolis rate is very simple in terms of its algorithm, but the convergence is not trivial. In following subsections, we show that the convergence for quite limited cases using a strong connectivity of the stochastic matrix.

A.3.1 Metropolis Matrix for the Model of the Size 2×2

We constructed the Metropolis matrix $\hat{M}^{[2,2]}(\beta)$ for the model of size $L_x = 2, L_z = 2$ in a concrete form and verified that all elements of the fourth power of the matrix are non-zero.

By the fact, we can see the existence of its unique stationary state as the long-time limit . In addition we investigated the distribution of the eigenvalues of $\hat{M}^{[2,2]}(\beta)$ for several temperatures and verified that the matrix $\hat{M}^{[2,2]}(\beta)$ has only an eigenvalue 1 and eigenvalue all inner than unit circle on the complex plane except for the case $\beta = 0$ (See Figure A.2).

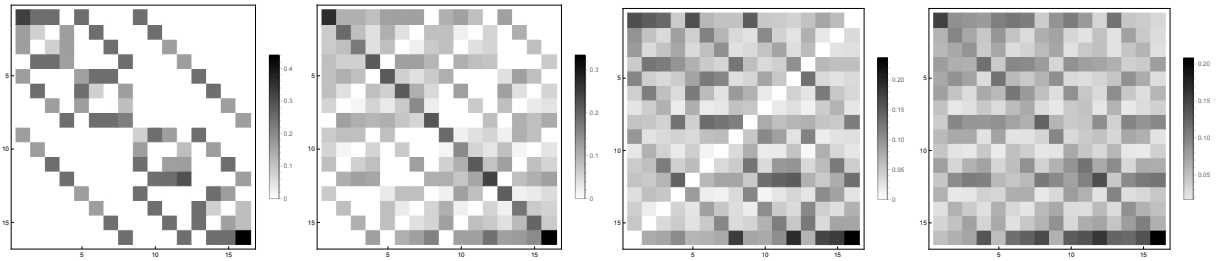

(a) $\hat{M}_{[2,2]}(\beta)$ (b) $\left\{\hat{M}_{[2,2]}(\beta)\right\}^2$ (c) $\left\{\hat{M}_{[2,2]}(\beta)\right\}^3$ (d) $\left\{\hat{M}_{[2,2]}(\beta)\right\}^4$

Figure A.1: The array plots of powers of $\hat{M}_{[2,2]}(\beta)$.

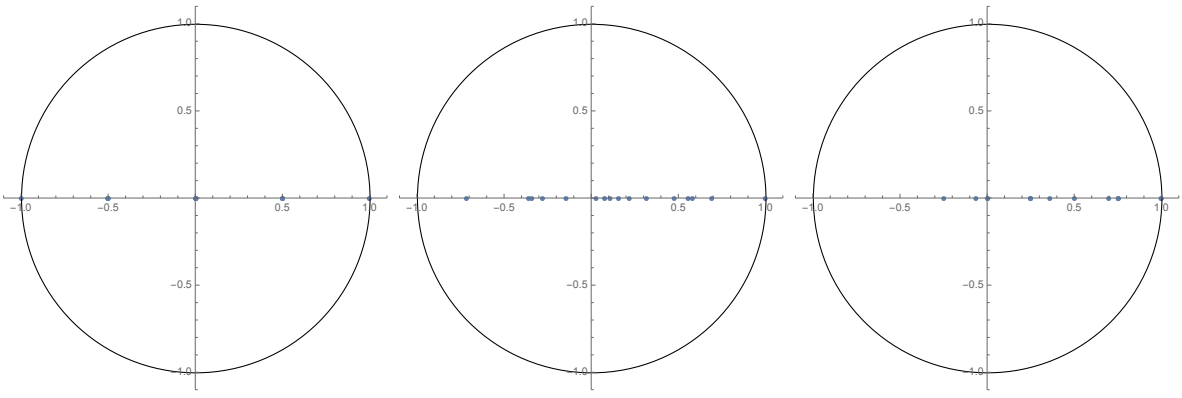

(a) $\beta = 0$ (b) $\beta = 0.1$ (c) $\beta = \infty$

Figure A.2: The distributions of eigenvalues for $\hat{M}^{[2,2]}(\beta)$.

Bibliography

[1] M. Weiss and F.-J. Elmer, Phys. Rev. B **53**, 7539 (1996).

[2] M. Weiss and F.-J. Elmer, Zeitschrift für Phys. B Condens. Matter **104**, 55 (1997).

[3] T. Strunz and F.-J. Elmer, Phys. Rev. E **58**, 1601 (1998).

[4] T. Strunz and F.-J. Elmer, Phys. Rev. E **58**, 1612 (1998).

[5] Q. Meng, L. Wu, D. O. Welch, and Y. Zhu, Phys. Rev. B **91**, 224305 (2015).

[6] A. D. Novaco, Phys. Rev. B **92**, 186301 (2015).

[7] Q. Meng, L. Wu, D. O. Welch, and Y. Zhu, Phys. Rev. B **91**, 224306 (2015).

[8] I. García-Mata, O. V. Zhirov, and D. L. Shepelyansky, Eur. Phys. J. D **41**, 325 (2007).

[9] E. Meyer, Science (80-.). **348**, 1089 (2015).

[10] A. Bylinskii, D. Gangloff, I. Counts, and V. Vuletić, Nat. Mater. **15**, 717 (2016).

[11] A. Dayo, W. Alnasrallah, and J. Krim, Phys. Rev. Lett. **80**, 1690 (1998).

[12] T. Novotný and B. Velický, Phys. Rev. Lett. **83**, 4112 (1999).

[13] N. Hosomi, A. Tanabe, M. Suzuki, and M. Hieda, Phys. Rev. B **75**, 064513 (2007).

[14] N. Hosomi and M. Suzuki, Phys. Rev. B **77**, 024501 (2008).

[15] N. Hosomi, J. Taniguchi, M. Suzuki, and T. Minoguchi, Phys. Rev. B **79**, 172503 (2009).

[16] M. Ternes, C. P. Lutz, C. F. Hirjibehedin, F. J. Giessibl, and A. J. Heinrich, Science (80-.). **319**, 1066 (2008).

[17] M. Urbakh and E. Meyer, Nat. Mater. **9**, 8 (2010).

[18] S. H. Kim, D. B. Asay, and M. T. Dugger, Nano Today **2**, 22 (2007).

[19] D. S. Grierson and R. W. Carpick, Nano Today **2**, 12 (2007).

[20] N. Manini, G. Mistura, G. Paolicelli, E. Tosatti, and A. Vanossi, Adv. Phys. X **2**, 569 (2017).

[21] D. Kadau, A. Hucht, and D. E. Wolf, Phys. Rev. Lett. **101**, 137205 (2008).

[22] M. P. Magiera, S. Angst, A. Hucht, and D. E. Wolf, Phys. Rev. B **84**, 212301 (2011).

[23] B. Wolter, Y. Yoshida, A. Kubetzka, S.-W. Hla, K. von Bergmann, and R. Wiesendanger, Phys. Rev. Lett. **109**, 116102 (2012).

[24] A. Hucht, Phys. Rev. E **80**, 061138 (2009).

[25] M. P. Magiera, L. Brendel, D. E. Wolf, and U. Nowak, EPL (Europhysics Lett. **87**, 26002 (2009).

[26] M. P. Magiera, L. Brendel, D. E. Wolf, and U. Nowak, EPL (Europhysics Lett. **95**, 17010 (2011).

[27] R. J. Glauber, J. Math. Phys. **4**, 294 (1963).